Correlation among the Ailaoshan–Song Ma–Song Chay orogenic belts and implications for the evolution of the eastern Paleo-Tethys Ocean

Yin Wang, Wei Lin, Michel Faure, Vuong van Nguyen, Lingtong Meng, Yang Chu, Wei Wei, Hoai Luong Thi Thu, Claude Lepvrier, Tich van Vu, et al.

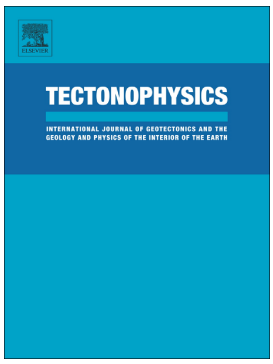

Correlation among the Ailaoshan–Song Ma–Song Chay orogenic belts and implications for the evolution of the eastern Paleo-Tethys Ocean

Yin Wang, Wei Lin, Michel Faure, Vuong Van Nguyen, Lingtong Meng, Yang Chu, Wei Wei, Hoai Luong Thi Thu, Claude Lepvrier, Tich Van Vu, Qiuli Li, Hao Wang, Zechao Chen, Lin Wu, Fei Wang

PII: S0040-1951(22)00412-7

DOI: https://doi.org/10.1016/j.tecto.2022.229618

Reference: TECTO 229618

To appear in: *Tectonophysics*

Received date: 26 May 2022

Revised date: 8 October 2022

Accepted date: 13 October 2022

Please cite this article as: Y. Wang, W. Lin, M. Faure, et al., Correlation among the Ailaoshan–Song Ma–Song Chay orogenic belts and implications for the evolution of the eastern Paleo-Tethys Ocean, *Tectonophysics* (2022), https://doi.org/10.1016/j.tecto.2022.229618

Correlation among the Ailaoshan–Song Ma–Song Chay orogenic belts and implications for the evolution of the eastern Paleo-Tethys Ocean

Yin Wang [a,b,c], Wei Lin [a,c] *, Michel Faure [d], Vuong Van Nguyen [e], Lingtong Meng [a,c], Yang Chu [a,c], Wei Wei [a,c], Hoai Luong Thi Thu [e], Claude Lepvrier [f], Tich Van Vu [e], Qiuli Li [a,c], Hao Wang [a,c], Zechao Chen [a,c], Lin Wu [a,c], Fei Wang [a,c]

a State Key Laboratory of Lithospheric Evolution, Institute of Geology and Geophysics, Innovation Academy of Earth Science, Chinese Academy of Sciences, Beijing 100029, China

b Geosteering & Logging Research Institute, Sinopec Matrix Corporation, Qingdao 266071, China

c College of Earth and Planetary Sciences, University of Chinese Academy of Sciences, Beijing 100049, China

d Institut des Sciences de la Terre d'Orléans, UMR CNRS 7327, Université d'Orléans, 45067 Orléans Cedex 2, France

e Faculty of Geology, Hanoi University of Science, Hanoi, Viet Nam

f Institut des Sciences de la Terre de Paris, UMR CNRS 7193, Case 129, Universit´e Pierre & Marie Curie, 75252 Paris Cedex 05, France

Abstract

The timing and mechanism of the combination between the South China Block (SCB) and the Indochina Block (IB) are controversial. Three ophiolitic mélange zones (Ailaoshan, Song Ma, and Song Chay) have been proposed as suture zones within this collisional orogen. However, the relationships among the three corresponding tectonic belts are unclear. In this study, we present detailed structural data for the three tectonic belts. The bulk architectures of the Ailaoshan, Song Ma, and Song Chay belts correlate well with one another. This similarity is also revealed by our new zircon U–Pb geochronological results from the Song Ma and Song Chay ophiolites. The regional deformation age is constrained to between 250 and 240 Ma by our new muscovite $^{40}Ar/^{39}Ar$ ages, and the medium-low temperature conditions are revealed by the quartz c-axis fabric. Considering the transformation effect of the Cenozoic large-scale sinistral strike-slip of the RRF and DBF, the Early Mesozoic Ailaoshan, Song Ma, and Song Chay suture zones should represent different segments of the same belt. Based on this hypothesis, we compiled the ages of the magmatism in this region, which allows us to propose an evolutional model as follows: i) ~380–310 Ma continental rifting and subsequent Ailaoshan–Song Ma–Song Chay ocean spreading as a branch of the Paleo-Tethys, ii) ~310–250 Ma oceanic subduction coeval with continental-arc magmatism, iii) ~250–240 Ma continental collision, iv) ~240–220 Ma post-collisional extension.

Key Words: Structural analysis, Ailaoshan–Song Ma–Song Chay, Paleo-Tethys, Indosinian orogeny

1. Introduction

Overprinting of older orogenies by younger orogenic events is common in the geological record, such as the Variscan orogenic belt superimposed by the Alpine orogenic event in Europe (e.g., Stampfli, 1996; Stampfli and Borel, 2002; Stampfli and Kozur, 2006; Faure et al., 2008) and the Laramide orogenic belt overprinted by the Cenozoic Sevier one in North America (e.g., Livaccari, 1991; Hodges et al., 1992; Livaccari and Perry, 1993; Aschoff and Steel, 2011; Weil and Yonkee, 2012). Therefore, the reconstruction of earlier orogenic belts should be undertaken with caution.

Southwestern China and northern Vietnam experienced polyphase deformation events, the most significant of which was the strike-slip motion related to Cenozoic extrusion of the southeastern part of the Indochina Block (Sundaland) owing to the collision between India and Eurasia (e.g., Tapponnier et al., 1990; Leloup et al., 1995). Another tectonic event is the so-called "Indosinian Movement" corresponding to the collision between the South China Block (SCB) and the Indochina Block (IB) (e.g., Depart, 1914, 1915; Fromaget, 1932, 1941; Lepvrier et al., 2011; Faure et al., 2014 and references therein). Despite the extensive Cenozoic tectonic overprint, a series of tectonic belts with mafic, ultramafic, and pelagic sedimentary blocks have been proposed as ophiolitic mélange zones, such as the Jingshajiang–Ailaoshan belt (Zhong, 1998; Sone & Metcalfe, 2008; Jian et al., 2009a, 2009b; Liu et al., 2011, 2012; Faure et al., 2014), the Song Ma belt (Trung et al., 2006; Nakano et al., 2008, 2010; Vượng et al., 2013; Zhang et al., 2013a; Shi et al., 2015; Ngo et al., 2016; Hieu et al., 2016; Wang et al., 2018; Zhou et al., 2020), and the Song Chay belt (Lepvrier et al., 2011; Faure et al., 2014; Wang et al., 2021a). To interpret the juxtaposition of several sutures and micro-blocks in the eastern Paleo-Tethys Ocean, an archipelagic-ocean model has been proposed (Liu et al., 1993, 2002; Pan et al., 1996). However, based on the structural analysis and regional tectonic understanding, another possibility has been proposed. Namely, the ophiolitic sutures between the SCB and IB (Jinshajiang, Ailaoshan, Song Ma, and Song Chay sutures) were connected as one suture zone in the Mesozoic, which was duplicated by the sinistral strike-slip faulting (Red River Fault and Dien Bien Fu Fault) in the Cenozoic to form the current juxtaposition of several suture zones in this region (Faure et al., 2014). Furthermore, the subduction direction of this branch of the Paleo-Tethys Ocean is still controversial: northward subduction (Lepvrier et al., 2008), southward subduction (Lepvrier et al.,

2011; Lin et al., 2011; Faure et al., 2014) and bidirectional subduction (Xu et al., 2019; Xia et al., 2020) have been suggested. In this study, based on the macrostructural and microstructural analyses, as well as previous and our new-geochronological data, we document the correlations between the Ailaoshan, Song Ma, and Song Chay ophiolitic mélange zones, and further constrain the opening and closure times of this branch of the Paleo-Tethys Ocean.

2. Geological setting

In southwestern China and northern Vietnam, the Indosinian Orogeny between the SCB and IB consists of three tectonic belts separated by the Red River fault (RRF) and Dien Bien Fu fault (DBF, Fig. 1), namely the Song Ma belt in SE, and the Song Chay belt in NE, and the Ailaoshan belt in NW (Lepvrier et al., 2008, 2011; Faure et al., 2014, 2016a, b, Li et al., 2021).

2.1. Song Ma belt

The Song Ma belt is situated in northwestern Vietnam bound to the NW and NE by the DBF and the RRF, respectively (Fig. 1). From SW to NE, several litho-tectonic units were identified: the Truong Son–Sam Nua zone, Song Ma ophiolitic mélange zone, inner zone, and outer zone (Figs. 1 and 2A, Li et al., 2021).

The Truong Son–Sam Nua zone is the widest part of the Song Ma belt, separated from the Song Ma ophiolitic mélange zone by the Cenozoic Song Ma fault (Figs. 1 and 2A). The Truong Son–Sam Nua zone is characterized by Permian to Triassic sedimentary-volcanic rocks, which unconformably overlie the Silurian sedimentary sequence and Carboniferous–Triassic (ca. 310–240 Ma) plutons. The plutons have low $^{87}Sr/^{86}Sr(i)$ and $\delta^{18}O$ values with high-$Mg^{\#}$ values and are I-type with positive ε_{Nd} (t) and ε_{Hf}(t) values (Qian et al., 2019).at the plutons developed in a continental-arc setting (Kamvong et al., 2014; Hoa et al., 2008). Therefore, the Truong Son–Sam Nua zone represents the magmatic arc related to the southwestward subduction of the Paleo-Tethys Ocean (e.g., Liu et al., 2012; Hieu et al., 2016; Wang et al., 2016, 2018; Hou et al., 2019; Qian et al., 2019; Li et al., 2021).

The Song Ma ophiolitic mélange zone consists of micaschist, deep marine sedimentary rocks, and sedimentary-volcanic rocks with blocks of serpentinized peridotite, gabbro, plagiogranite, diabase, basalt, and limestone enclosed (Trung et al., 2006; Vuong et al., 2013; Faure et al., 2014;

Zhang et al., 2014). The rocks in the Song Ma ophiolitic mélange zone underwent greenschist- to lower amphibolite-facies metamorphism (Zhang et al., 2014). Amphibolites and gabbros from the Song Ma ophiolitic mélange yield age ranges between 387 Ma and 313 Ma (Sm–Nd whole rock, Vuong et al., 2013). Along this zone in the northern Laos segment, zircon U–Pb ages from the plagioclase amphibolite yield a narrow range age of 367–356 Ma (Zhang et al., 2020). However, eclogite and high-pressure (HP) granulite-facies pelitic gneiss have been reported in this zone (Nakano et al., 2008, 2010; Zhang et al., 2013a, 2014). Zircons from the eclogite yielded a U–Pb age of 230.5 ± 8.2 Ma (Zhang et al., 2013a), and monazites from the HP granulite-facies pelitic gneiss yielded U–Th–Pb ages of 233–243 Ma (Nakano et al., 2008, 2010), which were interpreted as those of the syn-collisional metamorphism.

The inner zone, namely, the Nam Co zone (Fig. 1), is mainly composed of Neoproterozoic gneisses, micaschists, amphibolites, quartzite, marbles, and Paleozoic sandstone, siltstone, and limestone (e.g., Liu et al., 2012; Li et al., 2021). The rocks underwent greenschist- to amphibolite-facies metamorphism. Detrital zircon from this zone has revealed a dominant age peak at ~850 Ma (Hau et al., 2018; Zhou et al., 2020), which suggests that the inner zone belongs to the SCB. Biotite and muscovite along the inner zone have yielded $^{40}Ar/^{39}Ar$ ages of 250–240 Ma indicating a Triassic thermo–tectonic event (Lepvrier et al., 1997, 2004).

The outer zone is located between the inner zone and the RRF (Fig. 1). It consists of deformed and weakly metamorphosed Paleozoic sedimentary rocks. The most conspicuous rock types of the outer zone are the Late Permian ultramafic to mafic intrusive bodies and volcanic rocks, which are part of the Emeishan Large Igneous Province (ELIP; Chung et al., 1997; Wang et al., 2007; Balykin et al., 2010).

2.2. Song Chay belt

The Song Chay belt is located on the NE side of the RRF and extends to Yunnan and Guangxi provinces of China (Fig. 1). Similar to the Song Ma belt, several litho–tectonic zones are recognized, from the SW to NE, there are Day Nui Con Voi zone, Song Chay ophiolitic mélange zone, and the NE Vietnam thrust-and-nappe system (Wang et al., 2021a).

The Day Nui Con Voi zone is a Cenozoic large-scale antiformal complex geometrically

(Leloup et al., 1995; Nam et al., 1998; Wang et al., 1998, 2000; Anczkiewicz et al., 2007; Yeh et al., 2008). This zone is bounded by the RRF and the Song Chay Fault (SCF) to the SW and NE, respectively (Fig. 1). This unit is characterized by high-temperature metamorphic rocks (biotite–garnet–sillimanite micaschist, amphibolite, biotite-quartz schist), which were exhumed from the middle to lower crust along with the Cenozoic sinistral strike-slip of the RRF and the SCF (Leloup et al., 1995; Nam et al., 1998; Wang et al., 1998, 2000; Nakano et al., 2018).

The Song Chay ophiolitic mélange is distributed along the NE flank of the Day Nui Con Voi complex (Lepvrier et al., 2011; Faure et al., 2014; Wang et al., 2021a). The ultramafic and mafic rocks in the mélange lack accurate geochronological constraints. The depositional age of this mélange has been partly constrained to approximately 310–254 Ma by our previous analysis of detrital zircon from the ophiolitic mélange matrix (Wang et al., 2021a). The detrital zircon age distribution and the geochemistry suggest that the sandstone, which crops out as blocks in the Song Chay mélange matrix, originated from the SCB (Wang et al., 2021a). Additionally, the granitic plutons in NE Vietnam yielded Early Paleozoic to Late Mesozoic ages (Hoa et al., 2008; Chen et al., 2014; Roger et al., 2000, 2012; Yan et al., 2006; Gan et al., 2021); these plutons share similar geochemical characteristics and evolution process with those in the SCB.

The NE Vietnam thrust-and-nappe system is the widest zone in the Song Chay belt and can be subdivided into an inner zone and an outer zone by the Malipo fault (Fig. 1). Similar to the Song Ma belt, the inner zone, between the SCF and Malipo fault, consists of metamorphosed Neoproterozoic to Early Paleozoic sedimentary rocks, and the Song Chay augen gneiss massif. The rocks in the inner zone are characterized by pervasive ductile deformation and greenschist- to amphibolite-facies metamorphism (Maluski et al., 2001; Wang et al., 2021a). In contrast, on the NE side of the Malipo fault, the outer part of the nappe unit is characterized by weak ductilely deformed Late Paleozoic sedimentary rocks without significant metamorphism (Lepvrier et al., 2011). In the inner zone, the ages of metamorphism and deformation were constrained by various methods, such as zircon U–Pb age of 237 Ma (Yan et al., 2006), $^{40}Ar/^{39}Ar$ ages of 198–250 Ma (Maluski et al., 2001; Yan et al., 2006), and monazite U–Th–Pb ages of ~246 Ma (Gilley et al., 2003; Faure et al., 2014). The granitic plutons in the inner zone and outer zone have been dated by zircon U–Pb and yield ages between 87 and 428 Ma (Roger et al., 2000, 2012; Carter et al., 2001; Yan et al., 2006; Hoa et al., 2008; Chen et al., 2014). It is worth noting that the plutons older than

245 Ma are foliated and those younger than 245 Ma are undeformed (Chen et al., 2014).

However, in the northern Song Chay belt, the significant mafic and ultramafic zone named the Dian–Qiong zone was previously considered a "Suture Zone" as a branch of the Paleo-Tethys Ocean (Cai and Zhang, 2009). Halpin et al. (2016) interpreted the similar Song Hien Tectonic Zone as a segment of the Dian–Qiong zone in Vietnam. In this Dian–Qiong suture zone, 272–265 Ma mafic–ultramafic rocks were reported in the Babu area (Zhang et al., 2013b; Liu et al., 2018); Permian siliceous rocks were also found in this area (Feng and Liu, 2002). Furthermore, the mafic–ultramafic rocks from the Cao Bang area (Vietnam) yielded zircon U–Pb ages from 274–246 Ma (Halpin et al., 2016; Svetlitskaya et al., 2022). The geochemistry of the mafic–ultramafic rocks suggests both E-MORB and OIB features (Zhang et al., 2013b; Halpin et al., 2016; Liu et al., 2018; Svetlitskaya et al., 2022).

2.3. Ailaoshan belt

The Ailaoshan belt is located in southwestern Yunnan province, China (Fig. 1). Several NW–SE striking Cenozoic sinistral strike-slip faults divide this belt into narrow strips. The Ailaoshan belt is classically subdivided into four litho tectonic zones, from SW to NE: the Western Ailaoshan, Central Ailaoshan, Eastern Ailaoshan, and Jinping zones (Fig. 1, for details, see Zhong, 1998; Lai et al., 2014a, 2014b; Faure et al., 2016a).

The Western Ailaoshan zone is primarily composed of the Wusu and Yaxuanqiao volcanic sequences which are dominated by basalts (YNBGMR, 1982). The volcanic sequences are conformably overlain by Permian sandstone and limestone and underlain by Carboniferous sandstone and mudstone (Fan et al., 2010). The Wusu and Yaxuanqiao volcanic sequences yield zircon U–Pb ages of 288–246 Ma (Jian et al., 2009a, 2009b; Fan et al., 2010; Lai et al., 2014b). The geochemistry feature suggests both MORB and arc affinity (Fan et al., 2010; Lai et al., 2014b). Therefore, the Western Ailaoshan zone is recognized as a magmatic arc (Jian et al., 2009a, 2009b; Fan et al., 2010; Lai et al., 2014b; Faure et al., 2016a).

The Central Ailaoshan zone consists of ultramafic rocks, schist, chert, and exotic limestone blocks (YNBGMR, 1982; Zhong, 1998). The gabbro-diabase, and plagiogranite in this zone yield ages from 382.9 ± 3.9 Ma to 282.3 ± 5.8 Ma (Jian et al., 1998a, 1998b, 2009a; Zhong, 1998; Lai et

al., 2014a). Together with the MORB-like geochemistry of the mafic–ultramafic blocks (Lai et al., 2014a), the Central Ailaoshan zone is interpreted as the ophiolitic mélange zone and is commonly considered as the SE elongation of the Jingshajiang ophiolitic mélange zone (e.g., Zhong, 1998; Jian et al., 1998a, 1998b, 2009a, 2009b; Fan et al., 2010; Lai et al., 2014a; Faure et al., 2016a, 2016b). The depositional age of this mélange is constrained as Permo–Triassic (230–270 Ma) by our previous detrital zircon analysis from the ophiolitic mélange matrix (Li et al., 2021). The detrital zircon age distribution and the geochemistry suggest that the sandstone, which crops out as blocks in the Ailaoshan mélange matrix, is originated from either the IB or SCB (Li et al., 2021).

The Eastern Ailaoshan zone, also called the Ailaoshan complex, comprises migmatite, augen gneiss, paragneiss, amphibolite, marble, and granitic plutons (e.g., Leloup et al., 1995; Liu et al., 2011; Faure et al., 2016a). Zircons from these granitic plutons and gneiss yield ages between 750 and 850 Ma (Qi et al., 2012, 2014; Cai et al., 2014, 2015) and of approximately 240–250 Ma, respectively (Li et al., 2008; Qi et al., 2010). The pegmatite, leucogranite, and migmatite yielded zircon U–Pb ages of approximately 20–30 Ma (Schärer et al., 1990, 1994; Zhang and Schärer, 1999; Gilley et al., 2003; Sassier et al., 2009). Therefore, the Eastern Ailaoshan zone is the Neoproterozoic basement of the SCB that was subsequently involved in the Indosinian Orogeny (e.g., Liu et al., 2011; Faure et al., 2014). The final exhumation of the Eastern Ailaoshan zone is related to the sinistral strike-slip shearing along the RRF, coeval with the Cenozoic magmatism (e.g., Tapponnier et al., 1990; Leloup et al., 1995; Wang et al., 2020, 2021b).

The Jinping zone is a triangular wedge located in the southeastern Ailaoshan belt (Fig. 1) and connected to the outer zone in the Song Ma belt. Similar to the outer zone of the Song Ma belt, the Jinping zone consists of Ordovician–Carboniferous limestone, sandstone, and mudstone, and Late Permian mafic–ultramafic intrusive and volcanic rocks that were components of the ELIP(Xiao et al., 2004; Wang et al., 2007). Furthermore, the detrital zircon from the Silurian sandstone revealed an SCB affinity to the Jinping zone (Xia et al., 2016). Therefore, the Jinping zone is considered to represent the Paleozoic cover of the SCB (Xia et al., 2016).

3. Structural analysis

3.1. The bulk architecture of the Song Ma belt

The Truong Son–Sam Nua zone is characterized by a weakly deformed and non-metamorphosed Middle to Late Triassic sedimentary–volcanic series. The bulk architecture of this zone is dominated by NW–SE-trending open folds (Fig. 2A, 2C, 2D, and 2E). An axial planar slaty cleavage can only be observed locally. The NW–SE-trending upright folds are related to the Cenozoic strike-slip movement because the Jurassic and Cretaceous strata also have upright folds with vertical or sub-vertical NW–SE-trending axial planes.

The Song Ma ophiolitic mélange zone is separated from the Truong Son–Sam Nua zone by the Cenozoic Song Ma strike-slip fault (Fig. 2). The Song Ma zone consists of ultramafic, and mafic rocks, deep marine sedimentary rocks and granitoid blocks, which are enclosed in a highly sheared matrix (micaschist or pelitic schist). The foliations in the blocks are parallel to those in the matrix. The foliations in this zone strike NW–SE, and dip steeply to the NE or SW (Fig. 2A and 2E). Within these foliations, the NE–SW-trending mineral and stretching lineations are conspicuous (Figs. 2F and 3C). The bulk architecture of the Song Ma ophiolitic mélange zone is characterized by a series of tight NE-verging folds (Fig. 2C and 2D). Various kinematic criteria (shear bands, asymmetric quartz lenses) indicate a top-to-the-NE sense of shear (Fig. 3F).

The inner zone is represented by Neoproterozoic and Paleozoic sandstone, mudstone, and limestone that experienced a greenschist- to lower amphibolite-facies metamorphism (Faure et al., 2014). In this zone, the foliation is characterized by dominant NW–SE-trending with NE–SW-trending mineral and stretching lineation (Fig. 2F), and NE-warding tight folds are commonly developed (Fig. 3B). Some foliations in this zone are NE–SW-trending, which can be attributed to the DBF, especially east of the fault (Fig. 2A and 2F). It is worth noting that the NW–SE-trending lineations are especially well-developed along the Song Ma and Song La strike-slip faults (Fig. 2A and 2F). Indeed, these lineations are semi–penetrative, and more like striations; therefore, we consider them related to the Song Ma and Song La strike-slip faults. Generally, the bulk architecture of the inner zone is that of an NW–SE strike anticline. The kinematic indicators also suggest a top-to-the-NE shearing (Fig. 3D and 3E). It is worth noting that the deformation and metamorphism show a southwest-ward increasing grade in this zone, and eclogite and HP granulite-facies metapelite have been reported in this zone (Nakano et al., 2008, 2010; Zhang et al., 2013a, 2014).

The outer zone consists of weakly metamorphosed Paleozoic-Middle Triassic sedimentary

rocks, which are characterized by a series of NW–SE striking inclined folds and thrust faults. In this zone, weakly metamorphosed sandstone and siltstone were folded, verging to the NE, with associated meter-scale reverse faults (Fig. 3A). Metamorphic foliation and cleavage are locally developed along the faults, and sometimes along with NE-SW striking mineral and stretching lineation. From the kinematics view, the top-to-the-NE shearing and thrusting are widespread in this outer zone, together with a series of NW–SE striking folds with SW-dipping fold axial planes (Fig. 3B, 3C, and 3D); the outer zone can be regarded as a typical fold-and-thrust-belt within the orogenic belt.

3.2. The bulk architecture of the Song Chay belt

The Song Chay ophiolitic mélange zone cropped out as discontinuous patches upon the Paleozoic sequence along the SCF (Wang et al., 2021a; Fig. 4A). This zone is dominated by NW–SE-trending foliation and NE–SW-trending mineral and stretching lineation. Generally, the foliations in the Song Chay ophiolitic mélange are gently dipping with NE–SW-trending mineral and stretching lineations, although horizontal to subhorizontal NW–SE-trending semi-penetrative lineations or striations can be observed along the SCF. Therefore, the sheets of the mélange unit are interpreted as klippes thrusted upon the inner zone during the Indosinian Orogeny (Wang et al., 2021a).

The NE Vietnam thrust-and-nappe system is the widest zone in the Song Chay orogenic belt, stretching from northeastern Vietnam (NE side of the SCF) to the Youjiang basin in Guangxi province, China (Fig. 1). This zone has been recognized as the fold-and-thrust-belt in this orogenic belt (Lepvrier et al., 2011; Wang et al., 2021a; Yang et al., 2021). Comparable to the Song Ma belt, this wide thrust-and-nappe system can be subdivided into inner and outer zones by the Malipo fault (Figs. 1 and 4A). The inner zone, southwest of the Malipo fault, is characterized by pervasive ductile deformation and greenschist- to amphibolite-facies metamorphism (Fig. 4A). The metamorphic foliation of the inner zone is dominantly NW–SE-trending, along with the NE–SW-trending mineral and stretching lineations and isoclinal folds (Figs. 4 and 5). These kinematic indicators suggest a top-to-the-NE shearing (Fig. 5D, 5E, and 5F). It is worth noting that the Late Triassic conglomerate and sandstone are undeformed and unconformably overlie the deformed

Paleozoic sequences of this inner zone (Lepvrier et al., 2011; Wang et al., 2021a).

The outer zone, on the northeast side of the Malipo fault, extends to the Youjiang basin in China. It is characterized by the meter- to kilometer-scale folds and thrust faults. Although mylonitic foliation can be observed along the thrust faults, the rocks in the outer zone are weak or unmetamorphosed. Additionally, in the outer zone, deformation was progressively weaker from SW to NE and is characterized by meter-scale folds and thrusts in the Youjiang basin (Yang et al., 2021).

3.3. The bulk architecture of the Ailaoshan belt

In the Western Ailaoshan zone, the deformation and metamorphism are weak, and this zone is characterized by cleavage and brittle fractures (Fig. 6A, 6B, 6C, and 6D). The cleavage develops locally (Fig. 6C), dipping to the NE with a high angle (Fig. 7E). However, this cleavage can also be observed in the Late Triassic and Jurassic sedimentary rocks.

In contrast to the Western Ailaoshan zone, the deformation and metamorphism are much more intensive in the Central Ailaoshan zone. In this zone, the foliation and cleavage, dipping to the NE with a low angle, are pervasively developed. However, in most cases, the foliation and cleavage are nearly parallel, especially in the schist (Fig. 7C). Moreover, there are numerous NW–SE-trending tight folds with axial-plane cleavage (Fig. 7A), contemporary with the cleavage in the Western Ailaoshan zone. It is worth noting that this cleavage is widely developed in the Late Triassic sedimentary rocks (Fig. 7B). Two stages of mineral and stretching lineations can be found in this zone: one is NE–SW-trending and the other is NW–SE-trending (Fig. 6F). Parallel to the NE–SW-trending mineral and stretching lineations, the kinematic indicators mostly suggest a top-to-the-NE shearing (Fig. 7C and 7F, see also Faure et al., 2016a), with occasional top-to-the-SW shear indicators (Fig. 7D).

The Eastern Ailaoshan zone is characterized by NW–SE-trending foliation and NW–SE-trending mineral and stretching lineations (Fig. 6E). Along the SW boundary, the foliation dips to the NE, suggesting that the Eastern Ailaoshan zone thrusted upon the Central Ailaoshan zone. The bulk architecture of this zone is a series of folds, which support this interpretation (Fig. 6B, 6C, and 6D). The kinematic indicators in this zone suggest a top-to-the-NW shearing.

In the Jinping zone, the metamorphism was weak. The deformation is characterized by local cleavage and thrust faults, which dip to the SW (Fig. 6D). In the Early Paleozoic sequence, a kilometer-scale overturned fold can be inferred based on the inverted strata (Fig. 6D). Along the boundary of the Jinping zone and the Eastern Ailaoshan zone, the rocks of the Jinping zone have been extensively foliated and even mylonitized, and these rocks are characterized by NE-dipping foliation and NE–SW-trending lineation.

4. Estimation of the deformation temperature

To assess the deformation temperature, a quartz lattice-preferred orientation (LPO) analysis was carried out for c-axis orientation using a universal stage. A total of 12 samples from the three belts were selected, detailed information for these samples is listed in Table 1. Three samples (AS150, AS155, and AS161) were selected from the Central Ailaoshan ophiolitic mélange zone. Our samples experienced intensive ductile deformation and exhibit NE–SW-trending mineral and stretching lineations with top-to-the-NE kinematic indicators. Although the bulk architecture of the Central Ailaoshan zone has been superimposed by the Cenozoic southwest–ward thrust, which was characterized by NE-dipping cleavage (Figs. 6B, 6C, and 7B), we consider that the Cenozoic thrusting did not overprint the pre-Triassic deformation for the following two reasons: 1) the Cenozoic deformation that developed in the shadow crust cannot overprint the Indosinian ductile deformation that developed in the middle–lower crust; and 2) the selected samples from the Ailaoshan belt show a top-to-the-NE shearing in both field and thin–section observations, corresponding to the Indosinian deformation. Additionally, the selected samples of the Song Ma and Song Chay belts are from the inner and outer zones, where the superimposition of Cenozoic deformation is undetectable. Therefore, all 12 samples from the three tectonic belts can represent the Indosinian deformation.

The thin–sections of the selected samples were cut parallel to the X–Z principal strain plane in which the minimum principal strain axis (Z) is the pole of the pre-Triassic foliation, and the maximum principal strain axis (X) represents the NE–SW stretching lineations. In thin sections, the plagioclase grains are catalyzed or undeformed (Fig. 8A, 8F, 8G, 8H, and 8I). Quartz grains show textural evidence for crystal plastic deformation, characterized by undulose extinction,

dynamic recrystallization, and ribbon structures (Fig. 8). In the Song Ma belt, the elongated quartz grains defined the foliation (Fig. 8A, 8B, and 8C), some of the quartz grains are sigmoidal (Fig. 8B). The rigid plagioclase and garnet form porphyroblasts with elongated quartz as the tails, indicating a top-to-the-NE shearing (Fig. 8B). Quartz shows sweeping undulose extinction and dynamically recrystallized by bulging or subgrain rotation (Fig. 8A, 8B, and 8C). In the Ailaoshan belt, large elongated quartz grains show sweeping undulose extinction in a matrix of fine-grained muscovite and quartz (Fig. 8D, 8E, and 8F). The large quartz grains act as porphyroblasts and suggest a top-to-the-NE shear sense (Fig. 8D, 8E, and, -8F). Moreover, the tiny recrystallized quartz developed by bulging and subgrain rotation can also be observed (Fig. 8D, 8E, and, 8F). In the Song Chay belt, similar textures can also be observed. The porphyroblasts formed by rigid plagioclase and the shear band indicate a top-to-the-NE sense of shear (Fig. 8G, 8K, and 8L). Undulose extinction and subgrains can also be observed in the quartz grains.

All of our analyzed samples show asymmetrical point maxima in between the Z-axis and the Y-axis (Fig. 9). Most of the samples exhibit a point maximum close to the Z-axis, indicating a dominant basal <a> slip at low temperature (Law, 2014; Passchier and Trouw, 2005; Stipp et al., 2002). Sometimes scattered point maxima close to the Y-axis can be observed (e.g., TK136), this fabric is interpreted as a combination of basal <a> and rhomb <a> slip at medium-low temperatures (Passchier and Trouw, 2005). Therefore, the quartz c-axis fabrics of the chosen samples from the three tectonic belts all indicate a similar deformation mechanism characterized by a dominant basal <a> slip and a subordinate rhomb <a> slip. Therefore, our selected samples were deformed under medium- to low-temperature conditions (approximately 350–450 °C). It is also worth noting that the quartz c-axis fabric of these samples indicates a top-to-the-NE shearing (Fig. 9), consistent with the results of the field and microscopic observations. Our Ailaoshan results are consistent with the EBSD result of Fan et al. (2022).

5. Geochronological constraints

5.1. Zircon U–Pb dating

Owing to the lack of highly accurate geochronological data on the Song Ma and Song Chay ophiolites, the ages of the ophiolites could not be well constrained. Therefore, we selected four

samples from two ophiolitic zones for zircon secondary-ion mass spectrometry (SIMS) and laser-ablation inductively coupled plasma mass spectrometry (LA-ICPMS) U–Pb dating. The locations of these four samples are marked in Figs. 2 and 4.

The samples were processed by crushing, heavy liquid separation, and subsequent magnetic separation. Zircons were hand-picked and mounted in epoxy mounts, and then polished to section the crystals in half for analysis. The transmitted, as well as the reflected light, was used to avoid cracks and inclusions, and cathodoluminescence (CL) images, obtained from a CAMECA electron microscope, were used to identify the morphology and internal texture of the zircon grains.

SIMS zircon U–Pb isotope analyses for samples of the amphibolite-bearing granite, foliated granite, and metagabbro (21SM27, 21SM25A, and 18SM06 from the Song Ma belt) were measured by a CAMECA IMS-1280 at the Institute of Geology and Geophysics, Chinese Academy of Sciences (IGGCAS), Beijing. The instrument description and analytical procedure can be found in Li et al. (2009). The beam spot was 20 × 30-μm in size, and positive secondary ions were extracted with a 10-kV potential. Standard zircons (Qinghu, Plešovice; Sláma et al., 2008; Li et al., 2010) were used to determine the U–Th–Pb ratios and absolute abundances of the analyzed zircon. Concordia diagrams and ages were carried out using the Isoplot program (Ludwig, 2003). The detailed data are provided in Table S1.

Zircon U–Pb dating for the plagiogranite (TK235B from the Song Chay mélange zone) was performed using LA-ICP-MS at the IGGCAS. Laser ablation was operated at constant energy of 80 mJ and 10 Hz, with a 32-μm spot diameter. The highly purified He carrier gas-flow rate was 0.7 L/min; the Ar auxiliary gas-flow rate was 1.13 L/min. The total acquisition time of one spot was 45 s. The instrument description and analytical procedure can be found in Xie et al. (2008). Zircon 91500 and GJ-1 (Wiedenbeck et al., 1995; Jackson et al., 2004) were used as standards to normalize isotopic fractionation and calculate the U–Th–Pb ratios. The concordia diagram and age were carried out using the Isoplot program (Ludwig, 2003). The detailed data are provided in Table S1.

Sample 21SM27 from the Song Ma ophiolitic mélange zone is granite with amphibolite xenoliths and has a weakly magmatic foliation (Fig. 10A). Zircons from this sample are commonly euhedral and transparent, ranging from 100-μm to 150-μm in length with aspect ratios of 1:1–1:3. Most of them showed distinct oscillatory zoning and no inherited cores were detected

in the CL image (Fig. 10A). Twenty zircons were analyzed, yielding Th/U ratios of 0.26–1.18, indicated a magmatic origin. The concordant age of 244.6 ± 0.8 Ma [mean square weighted deviation (MSWD) = 0.17] is interpreted as the best estimate of the crystallization age of the granite.

Sample 21SM25A is a sheared granodiorite from the Song Ma ophiolitic mélange zone (Fig. 10B). Zircons from this sample are mostly euhedral, ranging from 150-μm to 300-μm in length with aspect ratios of 1:2–1:4. Most grains show typical magmatic growth zonation in the CL image, and some have inherited cores (Fig. 10B). Twenty zircons were analyzed, yielding Th/U ratios of 0.09–0.38. The concordant age of 264.4 ± 1.8 Ma (MSWD = 1.3) is interpreted as the best estimate of the crystallization age of this sample.

Sample 18SM06 is an intensively foliated metagabbro from the Song Ma ophiolitic mélange zone (Fig. 10C). Zircons from this sample are rare and small, ranging from 50-μm to 100-μm in length with aspect ratios of 1:1–1:3 (Fig. 10C). Twenty zircons were analyzed, yielding Th/U ratios of 0.02–0.97, and yielded ages from 261–818 Ma. Two concordant ages of 263.2 ± 2.3 Ma (MSWD = 1.6, n = 3) and 360.7 ± 3.0 Ma (MSWD = 0.26, n = 3) were obtained. The younger zircons are mostly euhedral and show typical magmatic growth zonation in the CL image (Fig. 10C); however, most zircons have a core–rim structure, and the older ages were obtained from the inherited cores (Fig. 10C). Therefore, we interpreted 263.2 ± 2.3 Ma as the best estimate of the crystallization age of this sample.

Sample TK235 is a lenticular plagiogranite from the Song Chay ophiolitic mélange zone (Fig. 10D). Only several tens of small zircon grains were acquired from seven kilograms of the sample. Zircons used in the analysis are mostly euhedral, ranging from 50-μm to 100-μm in length with aspect ratios of 1:1–1:3 (Fig. 10D). Eighteen zircons were analyzed, yielding ages of 339–740 Ma, among which nine results yielded a concordant age of 356.4 ± 2.9 Ma (MSWD = 4). This concordant age is interpreted as the crystallization age of this plagiogranite.

5.2. Muscovite $^{40}Ar/^{39}Ar$ dating

To constrain the deformation age of the NE Vietnam thrust-and-nappe stacks (Indosinian), two micaschists (TK161 and TK241) from the inner zone of the Song Chay belt were selected for

$^{40}Ar/^{39}Ar$ dating. The locations of the two samples are marked in Fig. 4. The micaschists are highly deformed, with NE–SW-trending lineations and a top-to-the-NE shearing in the field (Fig. 8I and 8K).

These two samples were crushed and sieved, and muscovite grains with 180–250 μm size were hand-picked under a binocular microscope and irradiated at the China Institute of Atomic Energy, China. The $^{40}Ar/^{39}Ar$ measurements were performed on an MM-5400 mass spectrometer at the $^{40}Ar/^{39}Ar$ and (U–Th)/He Laboratory, IGGCAS. A detailed analytical procedure was described by Wang et al. (2006). Weighted plateau, inverse isochron, and total fusion ages were calculated using the Ar-Ar-CALC software (Koppers, 2002), and the parameters for the calculation are the same as those in Wang et al. (2009). Age data are presented with 2-sigma uncertainties, and detailed analytical data are provided in Table S2.

TK161 yielded parent ages ranging from 243.1 Ma to 245.6 Ma, and gave a well-constrained plateau age of 244.7 ± 1.3 Ma, which is consistent with the inverse isochron age of 244.7 ± 1.5 Ma (Fig. 11). TK241 yielded parent ages ranging from 236.6 Ma to 241.4 Ma, and gave a well-constrained plateau age of 240.3 ± 1.6 Ma, which is consistent with the inverse isochron age of 240.2 ± 6.1 Ma (Fig. 11).

6. Discussion

6.1. Interpretation of the bulk architecture of the three tectonic belts

In the Song Ma belt, in terms of geodynamics, the Truong Son–Sam Nua zone represents the undeformed continental magmatic arc along the northeastern margin of the IB, the Song Ma ophiolitic mélange zone is the suture zone between the IB and SCB, the inner zone is the highly deformed and metamorphosed sedimentary rocks of the SCB involved in the subduction and exhumation processes, and the outer zone is the fold-and-thrust-belt developed in the sedimentary cover in the SCB (Fig. 2). Considering the bulk architecture of the four zones and their kinematics, we regard the Song Ma belt as a typical subduction to collisional orogenic belt between the IB and SCB, accommodated by the southwestward subduction of the SCB beneath the IB as proposed by most geologists (e.g., Liu et al., 2012; Faure et al., 2014).

In the Song Chay belt, from the view of tectonics, the NE Vietnam thrust-and-nappe system

is a fold-and-thrust-belt that accommodated large-scale shortening of the upper crust before the Late Triassic and recorded top-to-the-N(E) kinematics (Lepvrier et al., 2011; Faure et al. 2014; Wang et al., 2021a). In other words, the NE Vietnam thrust-and-nappe system is rooted in its southwestern part. Simultaneously, the Song Chay ophiolitic mélange zone was identified in the southwesternmost part, and geometrically on top of the nappe (Lepvrier et al., 2011; Wang et al., 2021a). The deformation turns intensive and metamorphism increases from northeast to southwest, along the mineral and stretching lineation direction. To the southwest, after passing through the Cenozoic Day Nui Con Voi unit (or Red River shear zone), the Song Da area did not record this tectonic event. Recently, it has been demonstrated that HP granulite and eclogite experienced early eclogite-facies metamorphism at 257 ± 8 Ma (Nakano et al., 2018), which suggests that there was a Late Permian subduction zone. All this evidence supports the Song Chay ophiolitic mélange as the original position, which can represent the location of the suture zone. Therefore, the Song Chay ophiolitic mélange zone is deemed to be the suture zone between the SCB and IB. According to the detrital zircon work from the Song Chay ophiolitic mélange, the magmatic arc, which is missing now, should have developed at approximately 310–250 Ma (Wang et al., 2021a). Considering approximately 500 km sinistral displacement along the RRF (Leloup et al., 1995), the possible magmatic arc of the Song Chay segment would have been displaced by the RRF, and might be hidden under the Red River delta and the South China Sea now (Fig. 1). Nevertheless, considering the subdivisions of each of the four zones and the related bulk architecture, the Song Chay belt exhibits strong similarities with the Song Ma belt. The remarkable consistency of geometric and kinematic features along the two sides of the so-called "Dian–Qiong suture" in the NE Vietnam thrust-and-nappe system seems to not support the "Dian–Qiong suture" as a suture zone between two individual blocks.

In the Ailaoshan belt, the NE-dipping cleavage in the Western and Central Ailaoshan zones, with the top-to-the-SW shearing, suggests southwestward thrusting (Fig. 6B and 6C). Because of the observation of the NE-dipping cleavage in the Late Triassic and Jurassic strata, we interpret the NE-dipping cleavage as a Cenozoic structure related to the strike-slip motion along the RRF with the Eastern Ailaoshan (the Ailaoshan complex) exhumed from the middle–lower crust and thrust upon the Central Ailaoshan zone (Fig. 6B and 6C). Despite the widespread Cenozoic deformation (Fig. 7B, 7D, and 7E), the pre-Late Triassic structures, ascribed to the Indosinian

Orogeny, can still be found in the Western and Central Ailaoshan zones, namely NE–SW-trending mineral and stretching lineations associated with top-to-the-NE kinematic indicators (Faure et al., 2016a). In the southwestern Ailaoshan belt, the Cenozoic deformation is expressed by brittle or brittle-ductile transformation deformation. The Early Mesozoic tectonic event, as mentioned in the discussion of the Song Ma and Song Chay Sections, has a distinct ductile deformation with greenschist-facies metamorphism. The deformations at different crustal levels allow us to separate the Mesozoic and Cenozoic deformations.

The geometry of the Ailaoshan belt has been significantly reworked by the Cenozoic strike-slip movement, however, the Indosinian architectures are partly preserved in the Jinping zone, which is considered to belong to the SCB (Faure et al., 2016b; Xia et al., 2016; Li et al., 2021). There, Paleozoic sedimentary rocks are folded and thrust toward the northeast. Although the folds have been partly reworked by SW-verging thrusting (Fig. 5D), we recognize it as a fold-and-thrust-belt, equivalent to the outer zone in the Song Ma belt.

Generally, the present-day bulk architecture of the Ailaoshan belt has been dramatically changed by the Cenozoic strike-slip deformation and transpressional structures (Leloup et al., 1995; Wang et al., 2021b). However, the Indosinian relics are partly preserved in the Jinping zone. According to our new structural data and the previous studies in this region, the Western and Central Ailaoshan zones, and the Jinping zone represent the magmatic arc, the suture zone, and the fold-and-thrust-belt of the pre-Late Triassic Indosinian Orogeny, respectively. The western part of the magmatic arc, corresponds with the southwestward subduction of the Paleo-Tethys Ocean, as does the Song Ma segment.

6.2. Geochronological constraints

The final collision between the SCB and IB is poorly constrained in the southwestern China–northern Vietnam region, especially in the Song Chay area. Previous works in the Song Chay belt give wide geochronological constraints between 198 Ma and 255 Ma from zircon and monazite U(Th)–Pb ages and amphibole, biotite, and muscovite $^{40}Ar/^{39}Ar$ ages (Fig. 12; Maluski et al., 2001; Gilly et al., 2003; Yan et al., 2006; Faure et al., 2014). In this study, we provide two well-

constrained muscovite $^{40}Ar/^{39}Ar$ ages of approximately 246–240 Ma from the Song Chay belt (Fig. 11). Usually the muscovite $^{40}Ar/^{39}Ar$ age represents the cooling age of the rocks, however, when the deformation temperature of the rock is close to the muscovite closure temperature and there is a no later high-temperature event in this area, the muscovite $^{40}Ar/^{39}Ar$ age can represent the deformation age.

According to the quartz LPO results of samples TK161 and TK241, the deformation occurred under medium–low temperatures (350–450 °C), consistent with the muscovite closure temperature (300–500 ℃). Moreover, in the Song Chay belt, the overprinting of Cenozoic shearing is localized along the SCF and is characterized by low-temperature deformation, away from the SCF, the Cenozoic strike-slip overprinting is inconspicuous (Wang et al., 2021a). However, the muscovite grains in both samples were sheared (Fig.8I and 8K), which may suggest that the $^{40}Ar/^{39}Ar$ ages may represent the cooling ages. The consistency in the deformation temperature and the closure temperature of muscovite suggests that the cooling age is very close to the deformation age. Therefore, we prefer to interpret the two $^{40}Ar/^{39}Ar$ plateau ages as the cooling ages of the rocks, which may be slightly younger or equivalent to the deformation age of the top-the-NE shearing.

The granite in the Song Ma ophiolite (21SM27) yields a 244.6 ± 0.8 Ma crystallization age. Although this granite is undeformed, a weakly magmatic foliation can be observed (Fig. 10A). Combined with the 246–240 Ma collisional age of the SCB and IB (Lepvrier et al., 1997, 2004), we interpret this granite as the results of syn–collisional magmatism.

The highly sheared granodiorite (21SM25A) yields a 264.4 ± 1.8 Ma crystallization age. Similar ages of diorite, plagiogranite, and gabbro have been reported in the Song Ma mélange (Hoa et al., 2008; Liu et al., 2012; Vuong et al., 2013; Hieu et al., 2016; Zhang et al., 2020), and these rocks were interpreted as evidence of arc-related magmatism (Hoa et al., 2008; Liu et al., 2012; Hieu et al., 2016; Zhang et al., 2020).

However, the gabbro (18SM06) yields two concordia ages, and the younger concordia age of 263.2 ± 2.3 Ma is interpreted as the crystallization age. A range of results from 290 Ma to 1867 Ma has been revealed in this sample, and we consider these zircons as inherited zircons. The older concordia age of 360.7 ± 3.0 Ma is similar to the ages reported from the plagioclase amphibolite and metagabbro in the Song Ma ophiolite (Vuong et al., 2013; Zhang et al., 2020). It is reasonable to consider that these older zircons were inherited from the older rocks in the Song Ma ophiolite,

therefore, we interpret the crystallization age of this gabbro to represent the age of this ophiolite.

The plagiogranite (TK235) in the Song Chay ophiolitic mélange zone yields a 356.4 ± 2.9 Ma crystallization age, which suggests that the Song Chay ophiolite crystallized at approximately 356.4 ± 2.9 Ma, and the Song Chay ocean was opened and developed with oceanic crust in the Early Carboniferous. Therefore, we interpret this age as the initial age of ocean spreading of the Song Chay ocean.

6.3. Correlations among the Ailaoshan, Song Ma, and Song Chay belts

According to our new structural data of the Ailaoshan, Song Ma, and Song Chay belts, three schematic profiles are shown in Fig. 13. Although the magmatic arc of the Song Chay belt is missing because of the Cenozoic strike-slip movement along the RRF, a similar tectonic zonation of the three tectonic belts can be determined. From SW to NE, there are three zones as follows: (i) a magmatic arc zone, formed by weakly deformed or undeformed sedimentary-volcanic sequences; (ii) an ophiolitic mélange zone; and (iii) a fold-and-thrust zone (inner and outer zones). The kinematic indicators in the ophiolitic mélange and fold-and-thrust zones of these three tectonic belts suggest a consistent top-to-the-NE shearing. The same southwestward subduction of the Paleo-Tethys Ocean can be inferred. Therefore, from the view of structural geology, the bulk architectures of the three tectonic belts correlate well with one another, although these three tectonic belts had been reworked by the Cenozoic strike-slip movement to varying degrees.

Our new zircon U-Pb age for the plagiogranite in the Song Chay ophiolitic mélange zone is 356.4 ± 2.9 Ma, which is interpreted as the emplacement age of the ophiolites. The reported ages from the Ailaoshan, Song Ma, and Song Chay ophiolitic mélange zones are summarized in Fig. 14. The 380–350 Ma age spans of the Ailaoshan and Song Ma ophiolites significantly overlap and are related to the initial continental rifting and ocean-basin spreading (Zhong, 1998; Jian et al., 1998a, 1998b; Jian et al., 2009b; Vuong et al., 2013; Lai et al., 2014a; Zhang et al, 2014; Zhang et al., 2020). Although only our data (356.4 ± 2.9 Ma) is provided in the Song Chay ophiolitic mélange, it is consistent with the ages reported for the Ailaoshan and Song Ma ophiolites. Therefore, the age consistency of the Ailaoshan, Song Ma, and Song Chay ophiolites indicates a good correlation among the three belts.

The quartz c-axis fabrics of 12 samples from the three tectonic belts yield similar patterns and suggest medium- to low-temperature conditions coeval with ductile shearing at approximately 350–450 °C, which is consistent with the muscovite $^{40}Ar/^{39}Ar$ closure temperature (300–500 °C). Therefore, our two muscovite $^{40}Ar/^{39}Ar$ plateau ages of the micaschist (TK161 and TK241) in the Song Chay belt can approximately represent the deformation age. In other words, the deformation characterized by the top-to-the-NE shearing in the Song Chay belt is constrained at around 245 Ma (Fig. 12). In the Song Ma belt, similar muscovite $^{40}Ar/^{39}Ar$ plateau ages of 253–237 Ma had been determined from the micaschist in the inner zone, among which two ages of 246 ± 4 Ma and 245.4 ± 4 Ma were well constrained (Fig. 12; Lepvrier et al., 1997). Combined with the medium- to low-temperature conditions revealed by the quartz c-axis fabrics, the deformation age of the Song Ma belt can be constrained at approximately 245 Ma, corresponding well to the ages from the Song Chay belt. Although there is no Mesozoic $^{40}Ar/^{39}Ar$ age reported in the Ailaoshan belt, the unmetamorphosed Late Triassic conglomerate unconformably overlies the highly deformed and metamorphosed micaschist suggesting that the deformation and metamorphism timings were earlier than the Late Triassic. The initial collision of the SCB and IB in the Ailaoshan belt was proposed at approximately 247 Ma (Fig. 12) and immediately followed by regional compressive deformation and high-grade metamorphism (Liu et al., 2015), which also agrees well with the Song Ma and Song Chay belt histories. Therefore, the Ailaoshan, Song Ma and Song Chay belts share similar medium to low-temperature deformation with a top-to-the-NE shearing at approximately 240–250 Ma. This striking consistency allows us to correlate them with one another.

Furthermore, the mafic–ultramafic rocks in the Jinping–Song Da region represents the inner part of the ELIP which was displaced by the RRF in the Cenozoic (Chung and Jahn, 1995; Xiao et al., 2004; Wang et al., 2007). The detrital zircons revealed that the inner zone and outer zone of the Song Ma belt belong to the SCB instead of the IB or the North Vietnam Terrane (Zhou et al., 2020).

The structural, chronological, and lithological similarities between the Ailaoshan, Song Ma, and Song Chay belts lead us to think that they connect and belong to the same collisional belt that separated the IB and SCB. Considering the Cenozoic large-scale sinistral strike-slip movements of the RRF and DBF, it is reasonable to consider the Jinping–Song Da region as a patch separated

from the SCB by the RRF and DBF. When considering the effect of the Cenozoic sinistral strike-slip movement of the DBF, we can infer that the Ailaoshan and Song Ma ophiolitic mélange zones were one connected mélange zone in the Mesozoic (Fig. 15A; points 1 and 2 could be connected if we omit the effect of the DBF, and the Ailaoshan and Song Ma ophiolitic mélange zones would merge into one). Furthermore, if we try to offset the 500–700 km sinistral strike-slip movement of the RRF (Leloup et al., 1995, 2007; Royden et al., 2008; Otofuji et al., 2012), the Ailaoshan–Song Ma ophiolitic mélange zone could be located in the southwestern Sichuan province, just between the Jinshajiang and the Song Chay ophiolitic mélange zones (Fig. 15A; the SW part of the RRF has been displaced by approximately 500–700 km and extruded to the SE, if we ignore the effect of the RRF, the united Ailaoshan–Song Ma mélange at **a'–b'** would be moved northwest–ward approximately 500–700 km, and this would put **a'** at **a** and **b'** at **b**. Under these conditions, the Ailaoshan–Song Ma ophiolitic mélange would fill the gap between the Jinshajiang and Song Chay ophiolitic mélanges). In this way, as already proposed (e.g., Faure et al, 2014), this branch of the Paleo-Tethys Ocean forms a single ocean between the SCB and IB (Fig. 15B).

6.4. Tectonic implications

The connection of the Ailaoshan–Song Ma–Song Chay belt allows us to investigate the Paleo-Tethys Ocean as a whole and reconstruct its evolution. We have compiled our geochronological data with the published data for this region (Fig. 16B). The ages from the ophiolitic mélange zones reveal a wide range from the Middle Devonian to Late Permian, formed by two age groups of 380–310 Ma and 270–260 Ma. According to previous studies, the 380–310 Ma plagiogranite and gabbro-diabase exhibit an N-MORB-like geochemical signature (Zhong, 1998; Jian et al., 1998b, 2009a; Vuong et al., 2013; Lai et al., 2014a; Zhang et al., 2014, 2020). These rocks are interpreted as associated with continental rifting and the subsequent ocean-basin spreading period (Zhong, 1998; Jian et al., 1998b, 2009a; Vuong et al., 2013; Lai et al., 2014a; Zhang et al., 2014, 2020). In contrast, the 270–260 Ma host rocks show arc-like or OIB-like geochemical signatures (Liu et al., 2012; Lai et al., 2014a; Zhang et al., 2014; Hieu et al., 2016), which were interpreted as related to the oceanic subduction (Liu et al., 2012; Vuong et al., 2013; Lai et al., 2014a; Zhang et al., 2014; Hieu et al., 2016). This evidence suggests that the Paleo-

Tethys Ocean opened in the Middle Devonian and closed in the Late Permian to Early Triassic. This hypothesis is consistent with the paleogeographic reconstructions based on multidisciplinary data (Zhong, 1998; Metcalfe, 1996, 2002, 2011, 2013, 2021; Sone and Metcalfe, 2008).

The magmatic rocks from the Western Ailaoshan and Truong Son–Sam Nua zones are considered the magmatic arc and yield ages ranging from 310 Ma to 220 Ma (e.g., Li et al., 2021). According to previous studies, the magmatic rocks of 310–240 Ma were the result of magmatism related to the southwestward subduction of the Paleo-Tethys Ocean (e.g., Fan et al., 2010; Liu et al., 2012; Lai et al., 2014b; Hieu et al., 2016; Wang et al., 2016, 2018; Hou et al., 2019; Qian et al., 2019). A magmatic gap at 270–265 Ma separates the arc-related magmatism into two groups (Fig. 13B). The earlier magmatism (310–270 Ma) is characterized by low $^{87}Sr/^{86}Sr(i)$ and $\delta^{18}O$ values, high-$Mg^{\#}$ values, and positive $\varepsilon_{Nd}(t)$ and $\varepsilon_{Hf}(t)$ values (e.g., Kamvong et al., 2014; Hieu et al., 2016; Qian et al., 2019), which suggests a significant mantle contribution (Kamvong et al., 2014; Hieu et al., 2016; Qian et al., 2019; Li et al., 2021). In contrast, the later magmatism (265–240 Ma) is dominated by peraluminous S-type granitoids with negative ε_{Nd} (t) and ε_{Hf} (t) values (Shi et al., 2015; Hieu et al., 2016; Wang et al., 2016; Qian et al., 2019; Hou et al., 2019), suggesting input from the continental crust (e.g., Shi et al., 2015; Hieu et al., 2016). Lastly, the 240–220 Ma magmatism is considered post-collisional. Therefore, the subduction of the Paleo-Tethys Ocean may have started at around 310 Ma and continued to around 250–240 Ma.

The timing of regional metamorphism and deformation was revealed by the metamorphic zircon U–Pb ages, monazite U–Th–Pb ages, and muscovite, biotite and amphibole $^{40}Ar/^{39}Ar$ ages ranges from 266–230 Ma, with the main group at 250–240 Ma (Fig. 15B). Considering the deformation age of 250–240 Ma as constrained by our $^{40}Ar/^{39}Ar$ ages, it is reasonable to consider that the collision between the SCB and IB occurred during this time. The eclogite and the HP pelitic gneiss in the Song Ma belt yielded ages of 233–230 Ma (Nakano et al., 2008; Zhang et al., 2013a), however, this can be interpreted as the exhumation age of the HP rocks.

Based on the information present in this work, the evolution of the Ailaoshan–Song Ma–Song Chay ocean is proposed in Fig. 16C. The Ailaoshan–Song Ma–Song Chay ocean was considered to have opened in the Middle Devonian (Zhong, 1998), followed by spreading in the 380–310 Ma period. The southwestward subduction of the Ailaoshan–Song Ma–Song Chay ocean under the IB may have started at approximately 310 Ma and continued to the Middle Triassic, as revealed by

the 310–240 Ma arc-related magmatism in the Western Ailaoshan–Truong Son zone. The magmatic gap at 270–265 Ma is related to the ELIP (Li et al., 2021). The collision of the SCB and IB may have started at approximately 250 Ma, followed by large-scale regional metamorphism and deformation that continued to approximately 240 Ma. After that, this region was dominated by the exhumation and cooling of HP rocks and magmatism associated with the post-collisional extension (Fig. 16C).

According to this tectonic model and the bulk architecture, the Paleo-Tethys Ocean was subducted southwestward beneath the IB and followed by the collision between the SCB and IB, which formed the well-known Indosinian Orogeny. However, the overall regional compressional structures in the SCB are mostly NE–SE-trending, which is best explained by the generally SW–NE-trending coastal Orogeny caused by the subduction of the Paleo-Pacific Ocean (Li and Li, 2007). Conversely, the fold-and-thrust belt of the Ailaoshan–Song Ma–Song Chay belt is restricted to the southwestern SCB, which means that the impact of the Indosinian Orogeny on the SCB is limited. According to the results of detrital zircon analysis from the matrix of the Ailaoshan–Song Ma–Song Chay ophiolitic mélanges, the SCB acted as a significant origin for the ophiolitic mélanges (Li et al., 2021; Wang et al., 2021a), which indicates that the Ailaoshan–Song Ma–Song Chay Ocean was relatively narrow. Based on that information, we speculate that the combination of the SCB and IB may be a soft docking, rather than a traditional head-on collision.

7. Conclusions

Based on our new structural, and geochronological data, and combined with the data from previous works in this region, the following four conclusions can be drawn:

(1) The bulk architectures of the Ailaoshan, Song Ma, and Song Chay tectonic belts correlate well with one other, although they had been reworked by the Cenozoic strike-slip movement to varying degrees.

(2) The temperature of the regional deformation constrained by the quartz c-axis fabric indicates medium-low temperature conditions (350–450 °C). Combined with our and previous muscovite $^{40}Ar/^{39}Ar$ ages, we constrain the collision time of the SCB and IB at 246–240 Ma.

(3) By removing the reworking effect of the Cenozoic RRF and DBF movements, we can

connect the Ailaoshan, Song Ma, and Song Chay suture zones.

(4) Combined with previous works, we propose a four-stage geodynamic evolution model of the Ailaoshan–Song Ma–Song Chay ocean: continental rifting at approximately 380–310 Ma, followed by ocean spreading; oceanic subduction of the Paleo-Tethys below IB at approximately 310–250 Ma; the continental collision between IB and SCB at approximately 250–240 Ma; post-collisional extension at approximately 240–220 Ma.

Acknowledgments

This work is supported by the National Nature Science Foundation of China (91855212) and the National Key R&D Program of China (Grant Numbers 2021YFB23013013, 2016YFC0600401). Prof. Zheng-Xiang Li, Prof. Ian Metcalfe, and one anonymous reviewer are acknowledged for their constructive comments and suggestions, which led to a great improvement of our manuscript.

During the review of this manuscript, on March 7th, we were shocked to learn that Claude Lepvrier (Pépé) passed away in Paris at 11h30. As a veteran of Indosinian orogen researcher and a leader in our work group, we deeply miss him and express our deepest condolences on his passing.

References

Anczkiewicz, R., Viola, G., Muentener, O., Thirlwall, M. F., Villa, I. M., Quong, N. Q., 2007. Structure and shearing conditions in the Day Nui Con Voi massif: Implications for the evolution of the Red River shear zone in northern Vietnam. Tectonics, 26(2), TC2001.

Aschoff, J., Steel, R., 2011. Anomalous clastic wedge development during the Sevier-Laramide transition, North American Cordilleran foreland basin, USA. Geol. Soc. Am. Bull.123,1822–1835.

Balykin, P.A., Polyakov, G.V., Izokh, A.E., Hoa, T.T., Phuong, N. T., Hung, T.Q., Petrova, T.E., 2010. Geochemistry and petrogenesis of Permian ultramafic-mafic complexes of the Jinping–Song Da rift (southeastern Asia). Russian Geol. Geophys. 51, 611–624.

Cai, J.X., Zhang, K.J., 2009. A new model for the Indochina and South China collision during the late Permian to the Middle Triassic. Tectonophysics 467 (1–4), 35–43.

Cai, Y.F., Wang, Y.J., Cawood, P.A., Fan, W.M., Li, H.C., Xing, X.W., Zhang, Y.Z., 2014. Neoproterozoic subduction along the Ailaoshan zone, South China: Geochronological and geochemical evidence from amphibolite. Precambrian. Res. 245, 13–28.

Cai, Y.F., Wang, Y.J., Cawood, P.A., Zhang, Y.Z., Zhang, A.M., 2015. Neoproterozoic crustal growth of the Southern Yangtze Block: geochemical and zircon U–Pb geochronological and Lu–Hf isotopic evidence of Neoproterozoic diorite from the Ailaoshan zone. Precambrian. Res. 266, 137–149.

Carter, A., Roques, D., Bristow, C., 2001. Understanding Mesozoic accretion in Southeast Asia: significance of Triassic themotectonism (Indosinian orogen) in Vietnam. Geology 29(3): 211–214.

Chen, Z., Lin, W., Faure, M., Lepvrier, C., Vuong, N. V., Tich, V. V., 2014. Geochronology and isotope analysis of the Late Paleozoic to Mesozoic granitoids from northeastern Vietnam and implications for the evolution of the South China block. J. Asian Earth Sci. 86, 131–150.

Chung, S.L., Jahn, B.M., 1995. Plume–lithosphere interaction in generation of the Emeishan flood basalts at the Permian–Triassic boundary. Geology 23 (10), 889–892.

Chung, S.L., Lee, T.Y., Lo, C.H., Wang, P.L., Chen, C.Y, Yem, N.T., Hoa, T.T., Wu, G., 1997. Intraplate extension prior to continental extrusion along the Ailao Shan–Red River shear

zone. Geology 25 (4), 311–314.

Deprat, J., 1914. Etude des plissements et des zones d'écrasement de la Moyenne et de la Basse Rivière Noire. Mémoire du Service Géologique de l'Indochine, Hanoi III, 59.

Deprat, J., 1915. Etudes géologiques sur la région septentrionale du Haut-Tonkin. Mémoire du Service Géologique de l'Indochine, Hanoi IV, 174.

Fan, W., Liu, J., Chen, X., Chen, W., Hou, C., Zhou, B., Dao, H.N., 2022. Formation of the Cenozoic Ailao Shan mid-crustal tectonic discontinuity: Role of Oligo-Miocene stratified sub-horizontal middle to lower crustal flow in the southeastern Tibetan Plateau. J. Struct. Geol. 153, 104464.

Fan, W.M., Wang, Y.J., Zhang, A.M., Zhang, F.F., Zhang, Y.Z., 2010. Permian arc-back-arc basin development along the Ailaoshan tectonic zone: geochemical, isotopic andgeochronological evidence from the Mojiang volcanic rocks, Southwest China. Lithos 119, 553–568.

Faure M., Lin W., Chu Y., Lepvrier C., 2016a. Triassic tectonics of the Ailaoshan Belt (SWChina): Early Triassic collision between the South China and Indochina Blocks, and Middle Triassic intracontinental shearing. Tectonophysics, 683, 27–42.

Faure, M., Bé Mézème, E., Cocherie, A., Rossi, P., Chemenda, A., Boutelier, D., 2008. Devonian geodynamic evolution of the Variscan Belt, insights from the French Massif Central and Massif Armoricain. Tectonics 27, TC2008.

Faure, M., Lepvrier, C., Nguyen, V.V., Vu, V.T., Lin, W., Chen, Z., 2014. The South China block-Indochina collision: where, when, and how? J. Asian Earth Sci. 79, 260–274.

Faure, M., Lin, W., Yang, C., Lepvrier, C., 2016b. Triassic tectonics of the southern margin of the South China Block. Compt. Rendus Geosci. 348, 5–14.

Feng, Q., Liu, B., 2002. Early Permian Radiolarians from Babu ophiolitic mélange in southeastern Yunnan. Earth Sci.-J. China Univ. Geosci. 27(1): 1–3.

Fromaget, J., 1932. Sur la structure des lndosinides. Comptes Rendus de l'Académie des Sciences, 195,1-53.

Fromaget, J., 1941. L'Indochine francaise, sa structure géologique, ses roches, ses mines et leurs relations possibles avec la tectonique. Bulletin Service Géologique de l'Indochine 26, 1-140.

Gan, C., Wang, Y., Zhang, Y., Qian, X., Zhang, A., 2021. The assembly of the South China and Indochina blocks: Constraints from the Triassic felsic volcanics in the Youjiang Basin. GSA

Bull. 133 (9/10), 2097–2112.

Gilley, L.D., Harrison, T.M., Leloup, P.H., Ryerson, F.J., Lovera, O.M., Wang, J.-H. 2003. Direct dating of left-lateral deformation along the Red River shear zone, China and Vietnam. J. Geophy. Res.: Solid Earth, 108(B2).

Halpin, J.A., Tran, H.T., Lai, C.K., Meffre, S., Crawford, A.J., Zaw, K., 2016. U–Pb zircon geochronology and geochemistry from NE Vietnam: a 'tectonically disputed' territory between the Indochina and South China blocks. Gondwana Res. 34, 254–273.

Hau, B.V., Kim, Y., Thanh, N.X., Hai, T.T., Yi, K., 2018. Neoproterozoic deposition and Triassic metamorphism of metasedimentary rocks in the Nam Co Complex, Song Ma Suture Zone, NW Vietnam. Geosci. J. 22(4), 549–568.

Hieu, P.T., Li, S.Q., Yu, Y., Thanh, N.X., Dung, L.T., Tu, V.L., Siebel, W., Chen, F., 2016. Stages of late Paleozoic to early Mesozoic magmatism in the Song Ma belt, NW Vietnam: evidence from zircon U–Pb geochronology and Hf isotope composition. Int. J. Earth Sci. 106 (3), 855–874.

Hoa, T.T., Anh, T.T., Phuong, N.T., Dung, P.T., Anh, T.V., Izokh, A.E., Borisenko, A.S., Lan, C.Y., Chung, S.L., Lo, C.H., 2008. Permo–Triassic intermediate-felsic magmatism of the Truong Son belt, eastern margin of Indochina. Compt. Rendus Geosci. 340, 112–126.

Hodges, K.A., Snoke, A.W., Hurlow, H.A., 1992. Thermal evolution of a portion of the Sevier hinterland in the northern Ruby Mountains—East Humboldt Range and Wood Hills, northeastern Nevada. Tectonics 11,154–164.

Hou, L., Liu, S., Guo, F., Xiong, F., Li, C., Shi, M., Zhang, Q., Xu, S., Wu, S., 2019. Geology, geochronology, and Hf isotopic composition of the Pha Lek Fe deposit, northern Laos: implications for early Permian subduction-related skarn Fe mineralization in the Truong Son belt. J. Earth Sci. 30, 109–120.

Jackson, S.E., Pearson, N.J., Griffin, W.L., Belousova, E.A., 2004. The application of laser ablation-inductively coupled plasma-mass spectrometry to in situ U-Pb zircon geochronology. Chem. Geol. 211, 47–69.

Jian, P., Liu, D., Kroner, A., Zhang, Q., Wang, Y., Sun, X., Zhang, W., 2009a. Devonian to Permian plate tectonic cycle of the Paleo-Tethys Orogen in southwest China (I): geochemistry of ophiolites, arc/back-arc assemblages and within-plate igneous rocks. Lithos

113, 748-766.

Jian, P., Liu, D., Kroner, A., Zhang, Q., Wang, Y., Sun, X., Zhang, W., 2009b. Devonian to Permian plate tectonic cycle of the Paleo-Tethys Orogen in southwest China (II): insights from zircon ages of ophiolites, arc/back-arc assemblages and within-plate igneous rocks and generation of the Emeishan CFB province. Lithos 113, 767–784.

Jian, P., Wang, X., He, L., Wang, C., 1998a. U–Pb zircon dating of the Shuanggou ophiolite from Xingping County, Yunnan Province. Acta Petrol. Sin. 14, 207–212 (in Chinese with English abstract).

Jian, P., Wang, X.F., He, L.Q., Wang, C.S., 1998b. Geochronology of ophiolite rocks from the Ailaoshan suture, Yunnan province, southwestern Yunnan province, southwestern China: implications of Palaeotethyan evolution. Geol. Miner. Resour. South China 1, 1–11 (in Chinese with English abstract).

Kamvong, T., Zaw, Khin, Meffre, S., Maas, R., Stein, H., Lai, C., 2014. Adakites in the Truong Son and Loei fold belts, Thailand and Laos: genesis and implications for geodynamics and metallogeny. Gondwana Res. 26, 165–184.

Koppers, A.A.P., 20002. ArArCALC-software for $^{40}Ar/^{39}Ar$ age calculations. Comput Geosci, 28(5), 605–619.

Lai, C.K., Meffre, S., Crawford, A.J., Zaw, K., Halpin, J.A., Xue, C.D., Salam, A., 2014a. The Central Ailaoshan ophiolite and modern analogs. Gondwana Res. 26, 75–88.

Lai, C.K., Meffre, S., Crawford, A.J., Zaw, K., Xue, C.D., Halpin, J.A., 2014b. The Western Ailaoshan Volcanic Belts and their SE Asia connection: a new tectonic model for the Eastern Indochina Block. Gondwana Res. 26, 52–74.

Law, R.D., 2014. Deformation thermometry based on quartz c-axis fabrics and recrystallization microstructures: a review. J. Struct. Geol. 66, 129–161.

Leloup, P.H., Lacassin, R., Tapponnier, P., Schärer, U., Zhong, D.L., Liu, X.H., Zhang, L.S., Ji, S.C., Phan, T.T., 1995. The Ailao Shan–Red River shear zone (Yunnan, China), tertiary transform boundary of Indochina. Tectonophysics 251, 3–84.

Leloup, P.H., Tapponnier, P., Lacassin, R., 2007. Discussion on the role of the Red River shear zone, Yunnan and Vietnam, in the continental extrusion of SE Asia. J. Geol. Soc. London 164, 1253–1260.

Lepvrier, C., Faure, M., Van Vuong, N., Van Vu, T., Lin, W., Thang, T.T., Phuong, T.H., 2011. North-directed Triassic nappes in Northeastern Vietnam (East Bac Bo). J. Asian Earth Sci. 41, 56–68.

Lepvrier, C., Maluski, H., Van Vuong, N., Roques, D., Axente, V., Rangin, C., 1997. Indosinian NW-trending shear zones within the Truong Son belt (Vietnam): ^{40}Ar-^{39}Ar Triassic ages and Cretaceous to Cenozoic overprints. Tectonophysics 283, 105–127.

Lepvrier, C., Maluski, H., Tich, V.V., Leyreloup, A., Thi, P.T., Vuong, N.V., 2004. The early Triassic Indosinian orogeny in Vietnam (Truong Son Belt and Kontum Massif); implications for the geodynamic evolution of Indochina. Tectonophysics 393, 87–118.

Lepvrier, C., Van Vuong, N., Maluski, H., Thi, P.T., Van Vu, T., 2008. Indosinian tectonics in Vietnam. Compt. Rendus Geosci. 340, 94–111.

Li, B.L., Ji, J.Q., Fu, X.R., Gong, J.F., Song, B., Qing, J.C., Zhang, C., 2008. Zircon SHRIMP dating and its geological implications of the metamorphic rocks in Ailao Shan–Diancang Mountain Ranges, west Yunnan. Acta Petrol. Sin 24, 2322–2330 (in Chinese with English abstract).

Li, Q., Lin, W., Wang, Y., Faure, M., Meng, L., Wang, H., Nguyen, V.V., Hoai, L.T.T., Lepvrier, C., Chu, Y., Wei, W., Vu, T.V., 2021. Detrital zircon U–Pb age distributions and Hf isotopic constraints of the Ailaoshan Song Ma Suture Zone and their paleogeographic implications for the Eastern Paleo-Tethys evolution. Earth Sci. Rev. 221.

Li, X.H., Liu, Y., Li, Q.L., Guo, C.H., Chamberlain, K.R., 2009. Precise determination of Phanerozoic zircon Pb/Pb age by multicollector SIMS without external standardization: Geochem. Geophys. Geosyst. v. 10, no. 4.

Li, X.H., Long, W., Li, Q., Liu, Y., Zheng, Y., Yang, Y., Chamberlain, K.R., Wan, D., Guo, C., Wang, X., Tao, H., 2010. Penglai Zircon megacrysts: A potential new working reference material for microbeam determination of Hf-O isotopes and U-Pb age. Geostand. Geoanal. Res. v.34, no. 2, p. 117–134.

Li, Z.X., Li, X.H., 2007. Formation of the 1300-km-wide intracontinental orogen and postorogenic magmatic province in Mesozoic South China: A flat-slab subduction model. Geology, v: 35, no. 2, p. 179–182.

Lin, W., Faure, M., Lepvrier, C., Chen, Z., Chu, Y., Wang, Q., Vuong, N.V., Tich, V.V., 2011. The

Early Mesozoic thrust-and-folds sheet structure along the southern margin of South China Block and its geodynamic. Chinese J. Geol. 46(1), 134–145. (in Chinese with English abstract).

Liu, B.P., Feng, Q.L., Chonglakman, C., Helmcke, D., 2002. Framework of Paleotethyan archipelago ocean of western Yunnan and its elongation towards north and south. Earth Sci. Front. 9 (3), 161–171 (in Chinese with English abstract).

Liu, B.P., Feng, Q.L., Fang, N.Q., Jia, J.H., He, F.X., 1993. Tectonic evolution of Paleao-Tethys poly-island-ocean in Changning-Menglian and Lancangjiang belts, southwestern Yunnan, China. J. Earth Sci. 18 (5), 529–539 (in Chinese with English abstract).

Liu, H., Peng, T., Guo, X., 2018. Geochronological and geochemical constraints on the coexistent N-MORB- and SSZ-type ophiolites in Babu area (SW China) and tectonic implications. J. Geol. Soc. 175 (4): 667–678.

Liu, H., Wang, Y., Cawood, P.A., Fan, W., Cai, Y., Xing, X., 2015. Record of Tethyan Ocean closure and Indosinian collision along the Ailaoshan suture zone (SW China). Gondwana Res. 27, 1292–1306.

Liu, J., Tang, Y., Song, Z., Tran, M.D., Zhai, Y., Wu, W., Chen, W., 2011. The Ailaoshan Belt in Western Yunnan: Tectonic Framework and Tectonic Evolution. J. Jilin Univ. (Earth Science Edition), 41(5), 1285–1303. (in Chinese with English abstract).

Liu, J.L., Tran, M., Tang, Y., Nguyen, Q.L., Tran, T.H., Wu, W., Chen, J., Zhang, Z., Zhao, Z., 2012. Permo-Triassic granitoids in the northern part of the Truong Son belt, NW Vietnam: geochronology, geochemistry and tectonic implications. Gondwana Res. 122, 628–644.

Livaccari, R.F., 1991. Role of crustal thickening and extensional collapse in the tectonic evolution of the Sevier-Laramide orogeny, western United States. Geology 19,1104–1107.

Livaccari, R.F., Perry, F.V., 1993. Isotopic evidence for preservation of Cordilleran lithospheric mantle during the Sevier-Laramide orogeny, western United States. Geology 21,719–722.

Ludwig, K.R., 2003, User's Manual for Isoplot 3.00: A Geochronological Toolkit for Microsoft Excel: Berkeley Geochronology Center Special Publication, v. 4, 70 p.

Maluski, H., Lepvrier, C., Jolivet, L., Carter, A., Roques, D., Beyssac, O., 2001. Ar^{40}-Ar^{39} and fission-track ages in the Song Chay Massif: Early Triassic and Cenozoic tectonics in northern Vietnam. Journal of Asian Earth Sciences 19, 233-248.

Metcalfe, I., 1996. Pre-cretaceous evolution of SE Asian terranes. In: Hall, R., Blundell, D. (Eds.), Tectonic Evolution of Southeast Asia, Geol. Soc. Spec. Publ, vol. 106, pp. 97–122.

Metcalfe, I., 2002. Permian tectonic framework and palaeogeography of SE Asia. J. Asian Earth Sci. 20 (6), 551–566.

Metcalfe, I., 2011. Palaeozoic-Mesozoic history of SE Asia. Geol. Soc. Spec. Publ. 355 (1), 7–35.

Metcalfe, I., 2013. Gondwana dispersion and Asian accretion: tectonic and palaeogeographic evolution of eastern Tethys. J. Asian Earth Sci. 66, 1–33.

Metcalfe, I., 2021. Multiple Tethyan Ocean basins and orogenic belts in Asia. J. Asian Earth Sci. 100, 87–130. https://doi.org/10.1016/j.gr.2021.01.012.

Nakano, N., Osanai, Y., Minh, N.T., Miyamoto, T., Hayasaka, Y., Owada, M., 2008. Discovery of high-pressure granulite-facies metamorphism in northern Vietnam: constraints on the Permo-Triassic Indochinese continental collision tectonics. Comptes Rendus Geosci. 340 (2–3), 127–138.

Nakano, N., Osanai, Y., Nam, N. V., Tri, T. V., 2018. Bauxite to eclogite: Evidence for late Permian supracontinental subduction at the Red River shear zone, northern Vietnam. Lithos, 302–303, 37–49.

Nakano, N., Osanai, Y., Sajeev, K., Hayasaka, Y., Miyamoto, T., Minh, N.T., Owada, M., 2010. Triassic eclogite from northern Vietnam: inferences and geological significance. J. Metamorph. Geol. 28, 59–76.

Nam, T. N., Toriumi, M., Itaya, T., 1998. P-T-t paths and post-metamorpic exhumation of the day nui con voi shear zone in vietnam. Tectonophysics, 290(3–4), 299–318.

Ngo, T.X., Santosh, M., Tran, H.T., Pham, H.T., 2016. Subduction initiation of Indochina and South China blocks: insight from the forearc ophiolitic peridotites of the Song Ma Suture Zone in Vietnam. Geol. J. 51, 421–442.

Vuong, V.N., Hansen, B.T., Wemmer, K., Lepvrier, C., Tích, V.V., Th˘a´ắng, T.T., 2013. U/Pb and Sm/Nd dating on ophiolitic rocks of the Song Ma suture zone (northern Vietnam): evidence for Upper Paleozoic Paleotethyan lithospheric remnants. J. Geodyn. 69, 140–147.

Otofuji, Y., Trung, V.D., Fujihara, M., Tanaka, M., Yokoyama, M., Kitada, K., Zaman, H., 2012. Tectonic deformation of the southeastern tip of the Indochina Peninsula during its southward displacement in the Cenozoic time. Gondwana Res. 22, 615–627.

Pan, G., Chen, Z., Li, X., Xu, Q., Jiang, X., 1996. Models for the evolution of the polyarcbasin systems in eastern Tethys. Sediment. Facies Palaeogeogr. 16 (2), 52–65 (in Chinese with English abstract).

Passchier, C.W., Trouw, R.A.J. (Eds.), 2005. Microtectonics. Springer, Berlin.

Qi, X.X., Zhu, L.H., Li, H.Q., Hu, Z.C., Li, Z.Q., 2010. Zircon LA-ICP-MS U–Pb dating for mylonitized granite from the Ailaoshan–Jinshajiang tectonic zone in the Eastern Qinghai–Tibet Plateau and its tectonic significance. Acta Geol. Sin. 84, 357–369 (in Chinese with English abstract).

Qi, X.X., Zeng, L.S., Zhu, L.H., Hu, Z.C., Hou, K.J., 2012. Zircon U–Pb and Lu–Hf isotopic systematics of the Daping plutonic rocks: implications for the Neoproterozoic tectonic evolution of the northeastern margin of the Indochina block, Southwest China. Gondwana Res. 21, 180–193.

Qi, X.X., Santosh, M., Zhu, L.H., Zhao, Y.H., Hu, Z.C., Zhang, C., Ji, F.B., 2014. MidNeoproterozoic arc magmatism in the northeastern margin of the Indochina Block, SW China: geochronological and petrogenetic constraints and implications for Gondwana assembly. Precambrian. Res. 245, 207–224.

Qian, X., Wang, Y., Zhang, Y., Zhang, Y., Senebouttalath, V., Zhang, A., He, H., 2019. Petrogenesis of the Permian–Triassic felsic igneous rocks along the Truong Son zone in northern Laos and their Paleotethyan assembly. Lithos 328–329, 101–114.

Roger, F., Leloup, P. H., Jolivet, M., Lacassin, R., Trinh, P. T., Brunel, M., Seward, D., 2000. Long and complex thermal history of the Song Chay metamorphic dome (Northern Vietnam) by multi-system geochronology. Tectonophysics, 321(4), 449–466.

Roger, F., Maluski, H., Lepvrier, C., Vu, V. T., Paquette, J. L., 2012. LA-ICPMS zircons U/Pb dating of Permo-Triassic and Cretaceous magmatisms in Northern Vietnam-Geodynamical implication. J. Asian Earth Sci. 48, 72–82.

Royden, L.H., Burchfiel, B.C., Van der Hilst, R.D., 2008. The geological evolution of the Tibetan Plateau. Science 321, 1054–1058.

Sassier, C., Leloup, P.H., Rubatto, D., Galland, O., Yue, Y., Lin, D., 2009. Direct measurement of strain rates in ductile shear zones: a new method based on syntectonic dikes. J. Geophys. Res. 114, B01406.

Schärer, U., Tapponnier, P., Lacassin, R., Leloup, P.H., Zhong, D.L., Ji, S.C., 1990. Intraplate tectonics in Asia: a precise age for large-scale Miocene movement along the Ailao Shan–Red River shear zone. China. Earth. Planet. Sci. Lett. 97 (1), 65–77.

Schärer, U., Zhang, L.S., Tapponnier, P., 1994. Duration of strikeslip movements in large shear zones: The Red River belt. China. Earth. Planet. Sci. Lett. 126, 379–397.

Sláma, J., Košler, J., Condon, D.J., Crowley, J.L., Gerdes, A., Hanchar, J.M., Horstwood, M.S.A., Morris, G.A., Nasdala, L., Norberg, N., Schaltegger, U., Schoene, B., Tubrett, M.N., Whitehouse, M.J., 2008. Plešovice zircon — A new natural reference material for U–Pb and Hf isotopic microanalysis. Chem. Geol., v. 249, no. 1–2, p. 1-35.

Shi, M.F., Lin, F.C., Fan, W.Y., Deng, Q., Cong, F., Tran, M.D., Zhu, H.P., Wang, H., 2015. Zircon U–Pb ages and geochemistry of granitoids in the Truong Son terrane, Vietnam: tectonic and metallogenic implications. J. Asian Earth Sci. 101, 101–120.

Sone, M., Metcalfe, I., 2008. Parallel Tethyan sutures in mainland Southeast Asia: New insights for Palaeo-Tethys closure and implications for the Indosinian orogeny. Compt. Rendus Geosci. 340, 166–179.

Stampfli, G.M., 1996. The Intra-Alpine terrain: a Paleotethyan remnant in the Alpine Variscides. Eclogae geol. Helv. 89(1), 13–42.

Stampfli, G.M., and Borel, G.D., 2002. A plate tectonic model for the Paleozoic and Mesozoic constrained by dynamic plate boundaries and restored synthetic oceanic isochrons. Earth Planet. Sci. Lett. 196 (1–2), 17–33.

Stampfli, G.M., and Kozur, H., 2006. Europe from the Variscan to the Alpine cycles. In: Gee, D.G., and Stephenson, R. (eds) European Lithosphere Dynamics. Geological Society, London, Memoirs, 32, 57–82.

Stipp, M., Stünitz, H., Heilbronner, R., Schmid, S.M., 2002. The eastern Tonale fault zone: a 'natural laboratory' for crystal plastic deformation of quartz over a temperature range from 250 to 700 °C. J. Struct. Geol. 24, 1861–1884.

Svetliskaya, T.V., Ngo, T.H., Nevplko, P.A., Tran, T.A., Izokn, A.E., Shelepaev, R.A., Tran, T.H., Ngo, T.P., Fominykh, P.A., Pham, N.C., 2022. Zircon U–Pb ages of Permian-Triassic igneous rocks in the Song Hien structure, NE Vietnam: The Emeishan mantle plume or the Indosinian orogeny? J. Asian Earth Sci. 224, 105033.

Tapponnier, P., Lacassin, R., Leloup, P. H., Scharer, U., Zhong, D., Wu, H., Liu, X., Ji, S., Zhang, L., Zhong, J., 1990, The Ailao Shan–Red River metamorphic belt: tertiary left-lateral shear between Indochina and South China. Nature, 343(6257), 431–437.

Trung, N., Tsujimori, T., Itaya, T., 2006. Honvang serpentinite body of the Song Ma fault zone, Northern Vietnam: a remnant of oceanic lithosphere within Indochina and South China suture. Gondwana Res. 9, 225–230.

Wang, C.Y., Zhou, M.F., Qi, L., 2007. Permian flood basalts and mafic intrusions in the Jinping (SW China)–Song Da (northern Vietnam) district: mantle sources, crustal contamination and sulfide segregation. Chem. Geol. 243, 317–343.

Wang, E.C., Fan, C., Su, Z., 2021b. Deformation and sedimentary responses to top-to-north shear along the range front of the Big Bend of the Ailao Shan – Red River shear zone, SE edge of the Tibetan Plateau, and its tectonic implications. Tectonics, e2021TC007067.

Wang, F., He, H.Y., Zhu, R.X., Sang, H.Q., Wang, Y.L., Yang, L.K., 2006. Intercalibration of internatioal and domestic $^{40}Ar/^{39}Ar$ dating standards. Science China–Earth Sci. 49, 461–470.

Wang, F., Zheng, X.S., Lee, J.I.K., Cho, Y.H., Evans, N., Zhu, R.–X., 2009. An $^{40}Ar/^{39}Ar$ geochronology on a mid-Eocene igneous event on the Barton and Weaver peninsulas: implications for the dynamic setting of the Antarctic Peninsula. Geochem. Geophys. Geosyst. 10.

Wang, P.L., Lo, C.H., Chung, S.L., Lee, T.–Y., Lan, C.Y., Thang, T. V., 2000. Onset timing of left-lateral movement along the Ailao Shan–Red River Shear Zone: $^{40}Ar/^{39}Ar$ dating constraint from the Nam Dinh Area, northeastern Vietnam. J. Asian Earth Sci. 18(3), 281–292.

Wang, P.L., Lo, C.H., Chung, S.L., Lee, T.Y., Lan, C.Y., Yem, N. T., 1998. Thermochronological evidence for the movement of the Ailao Shan–Red River shear zone: A perspective from Vietnam. Geology, 26(10), 887–890.

Wang, S., Mo, Y., Wang, C., Ye, P., 2016. Paleotethyan evolution of the Indochina Block as deduced from granites in northern Laos. Gondwana Res. 38, 183–196.

Wang, Y., Lin, W., Faure, M., Lepvrier, C., Chu, Y., Nguyen, V.V., Hoai, L.T.T., Wei, W., Liu, F., Vu, T.V., 2021a. Detrital zircon U–Pb age distribution and Hf isotopic constraints from the terrigenous sediments of the Song Chay Suture Zone (NE Vietnam) and their paleogeographic implications on the Eastern Paleo-Tethys evolution. Tectonics, 40,

e2020TC006611.

Wang, Y., Qian, X., Cawood, P.A., Liu, H., Feng, Q., Zhao, G., Zhang, Y., He, H., Zhang, P., 2018. Closure of the East Paleotethyan Ocean and amalgamation of the Eastern Cimmerian and Southeast Asia continental fragments. Earth Sci. Rev. 186, 195–230.

Wang, Y., Wang, Y., Schoenbohm, L.M., Zhang, P., Zhang, B., Sobel, E.R., Zhou, R., Shi, X., Zhang, J., Stockli, D.F., Guo, X., 2020. Cenozoic Exhumation of the Ailaoshan–Red River Shear Zone: New Insights from Low-Temperature Thermochronology. Tectonics, 39(9), e2020TC006151.

Weil, A.B., Yonkee, W.A., 2012. Layer-parallel shortening across the Sevier fold-thrust belt and Laramide foreland of Wyoming: spatial and temporal evolution of a complex geodynamic system. Earth Planet. Sci. Lett. 357–358, 405–420.

Wiedenbeck, M., All´e, P., Corfu, F., Criffin, W.L., Meier, M., Oberli, F., Von Quadt, A., Roddick, J.C., Spiegel, W., 1995. Three natural zircon standards for U-Th-Pb, Lu-Hf, trace-element and REE analyses. Geostand. Newslett. 19, 1–23.

Xia, X., Xu, J., Huang, C., Long, X., Zhou, M., 2020. Subduction polarity of the Ailaoshan Ocean (eastern Paleotethys): constraints from detrital zircon U–Pb and Hf–O isotopes for the Longtan Formation. Geol. Soc. Am. Bull. 132, 987–996.

Xiao, L., Xu, Y.G., Mei, H.J., Zheng, B., Pirajno, F., 2004. Distinct mantle sources of low-Ti and high-Ti basalts from the western Emeishan large igneous province, SW China: implications for plume-lithosphere interaction. Earth Planet. Sci. Lett. 228, 525–546.

Xie, L., Zhang, Y., Zhang, H., Sun, J., Wu, F., 2008. In situ simultaneous determination of trace elements, U–Pb and Lu–Hf isotopes in zircon and baddeleyite. Chinese Sci. Bull. 53(10), 1565–1573.

Xu, J., Xia, X., Lai, C., Long, X., Huang, C., 2019. When did the paleotethys Ailaoshan ocean close: new insights from detrital zircon U–Pb age and Hf isotopes. Tectonics 38, 1798–1823.

Yan, D.P., Zhou, M.F., Wang, C. Y., Xia, B., 2006. Structural and geochronological constraints on the tectonic evolution of the Dulong–Song Chay tectonic dome in Yunnan province, SW China. J. Asian Earth Sci. 28(4–6), 332–353.

Yang, W.-X., Yan, D.P., Qiu, L., Wells, M.L., Dong, J.M., Gao, T., Zhang, Z., Mu, H., Wang, X., Wang, F., 2021. Formation and forward propagation of the Indosinian foreland fold-thrust

belt and Nanpanjiang foreland basin in SW China. Tectonics, 40, e2020TC006552.

Yeh, M.W., Lee, T.Y., Lo, C.H., Chung, S.L., Lan, C.Y., Anh, T. T., 2008. Structural evolution of the Day Nui Con Voi metamorphic complex: Implications on the development of the Red River Shear Zone, Northern Vietnam. J. Struct. Geol. 30(12), 1540–1553.

YNBGMR (Bureau of Geology and Mineral Resources–Yunnan), 1982. Regional Geology of Guangxi Zhuang Autonomous Region. Geological Memoirs, Series 1, 3, 737pp.

Zhang, B., Ding, J., Zhang, L., Zhang, B., Chen, M., 2013b. SHRIMP zircon U–Pb chronology of the Babu ophiolite in southeastern Yunnan Province. Acta Geol. Sin. 87(10): 1498–1509.

Zhang, L.S., Schärer, U., 1999. Age and origin of magmatism along the Cenozoic Red River shear belt, China. Contrib. Miner. Petrol. 134, 67–85.

Zhang, R.Y., Lo, C.H., Chung, S.L., Grove, M., Omori, S., Iizuka, Y., Liou, J.G., Tri, T.V., 2013a. Origin and Tectonic Implication of Ophiolite and Eclogite in the Song Ma Suture Zone between the South China and Indochina Blocks. J. Metamorph. Geol. 31 (1), 49–62.

Zhang, R.Y., Lo, C.H., Li, X.H., Chung, S.L., Anh, T.T., Tri, T.V., 2014. U–Pb dating and tectonic implication of ophiolite and metabasite from the Song Ma suture zone, Northern Vietnam. Am. J. Sci. 314, 649–678.

Zhang, Y., Yang, X., Wang, Y., Qian, X., Wang, Y., Gou, Q., Senebouttalath, V., Zhang, A., 2020. Rifting and subduction records of the Paleo-Tethys in North Laos: Constraints from Late Paleozoic mafic and plagiogranitic magmatism along the Song Ma tectonic zone. GSA Bull. 133, 212–232.

Zhong, D., 1998. The Paleotethys Orogenic Belt in West of Sichuan and Yunnan. Science Publishing House, Beijing (in Chinese).

Zhou, X., Yu, J.H., Sun, T., Wang, X., Tran, M. D., Nguyen, D., 2020. Does Neoproterozoic Nam Co formation in Northwest Vietnam belong to South China or Indochina? Precambrian Res. 337. https://doi.org/10.1016/j.precamres.2019.105556

Yin Wang: Investigation, Formal analysis, Data curation, Writing - original draft, Writing - review & editing, Visualization.

Wei Lin: Conceptualization, Supervision, Methodology, Investigation, Data curation, Funding acquisition, Writing - review & editing.

Michel Faure: Investigation, Writing - original draft, Writing - review & editing

Vuong Van Nguyen: Investigation, Writing - original draft, Writing - review & editing.

Lingtong Meng: Formal analysis, Data curation, Writing - review & editing

Yang Chu: Methodology, Writing - review & editing

Wei Wei: Methodology, Writing - review & editing

Hoai Luong Thi Thu: Investigation.

Claude Lepvrier: Writing - original draft

Tich Van Vu: Investigation.

Qiuli Li: Methodology

Hao Wang: Methodology

Zechao Chen: Investigation, Formal analysis, Data curation

Lin Wu: Methodology

Fei Wang: Methodology

No conflict of interest exits in the submission of this manuscript. All the authors listed have approved the manuscript that is enclosed. Neither the entire paper nor any part of its content has been published or has been accepted elsewhere. It is not being submitted to any other journal at the same time.

Table 1 Selected samples for quartz c-axis fabrics analysis

Sample Name	GPS Coordinate	lithology	Tectonic position
18SM07	20.920488°N, 103.970311°E	Quartz schist	Song Ma belt- ophiolitic mélange zone
18SM10	21.037361°N, 103.98159°E	Garnet-quartz schist	Song Ma belt- inner zone
21SM24	21.297240°N, 103.4185°E	Quartz schist	Song Ma belt- inner zone
AS150	23.7116°N, 101.6715°E	Mylonite	Ailaoshan belt-Central Ailaoshan zone
AS155	23.7143°N, 101.6731°E	Mylonite	Ailaoshan belt-Central Ailaoshan zone
AS161	23.9549°N, 101.5082°E	Mylonite	Ailaoshan belt-Central Ailaoshan zone
TK92	22.643933°N, 105.8463°E	Mylonite	Song Chay belt-outer zone
TK136	22.909217°N, 104.8596°E	Granitic gneiss	Song Chay belt-inner zone
TK161	22.6113°N, 105.4848°E	Quartz schist	Song Chay belt-inner zone
TK195	22.231483°N, 105.23375°E	Quartz schist	Song Chay belt-inner zone
TK241	22.287983°N, 104.428167°E	Mica-quartz schist	Song Chay belt-ophiolitic mélange
TK242	22.292533°N, 104.434933°E	Mica-quartz schist	Song Chay belt-inner zone

Fig.1. (A) Tectonic outline of east Asia (modified from Lin et al., 2008). (B) Tectonic map of Southwest China-North Vietnam region, modified from the 1:1500000 Geological map of the five countries of southeast Asia and adjacent areas (Chengdu Institute of Geology and Mineral Resources, 2006). Nam Co: Neoproterozoic sedimentary rocks deformed and metamorphosed in Triassic during the “Indosinian” SW subduction and subsequent NE-ward thrusting; SC: Song Chay massif; ALMZ: Ailaoshan mélange zone; SMMZ: Song Ma mélange zone; SCMZ: Song Chay mélange zone; RRF: Red River fault; SCF: Song Chay fault; DBF: Dien Bien Phu fault; SD: Song Da belt; WALB: western Ailaoshan belt; JP: Jinping zone.

Fig. 2. (A) Geological and structural map of the Song Ma belt with the sampling sites. (B-E) Cross sections through the Song Ma belt with locations marked in (A). (F-H) Stereographic projections of the foliations, lineations and beddings for the ophiolitic mélange zone, inner zone and outer zone of the Song Ma belt (N: number of the measurements; Schmidt net, lower hemisphere).

Fig. 3. Field-scale photographs of Song Ma belt. (A) Recumbent fold in the Outer zone (21.2153°N, 104.330383°E). (B) Tight fold in the Inner zone (21.518517°N, 103.1372°E). (C) Micaschist with NE-SW trending lineation in the Inner zone (21.800117°N, 103.2939°E). (D) Sheared calcite veins in limestone in the Inner zone, suggesting a top-to-the-NE shearing (21.62055°N, 103.5032°E). (E) Sigmoid clast in the sheared carbonite indicating a top-to-the-NE kinematics (21.58295°N, 103.409783°E). (F) Microscopic photo a garnet-bearing quartz schist in the Inner zone, indicating a top-to-the-NE sense of shear (21.037361°N, 103.93159°E).

Fig. 4. (A) Geological and structural map of the Song Chay belt with the sampling sites. (B-E) Cross sections through the Song Chay belt with locations marked in (A). (F-G) Stereographic projections of the foliations, and lineations for the ophiolitic mélange zone, inner zone and outer zone of the Song Chay belt (N: number of the measurements; Schmidt net, lower hemisphere).

Fig. 5. Field and micro-scale photographs of Song Chay belt. (A) NE-verging fold with axial planar crenulation cleavage in the micaschist and quartz vein, Inner zone (21.82625°N, 105.27505°E). (B) NE-verging fold and thrust fault in the limestone, Inner zone (23.240417°N, 105.411867°E). (C) Quartzo-schist with NE-SW trending lineation, Inner zone (22.367233°N, 105.415383°E). (D) Sigmoidal plagioclase porphyroclast and quartz with pressure shadow top-to-the-NE shearing in metapelite, Inner zone (22.500717°N, 105.815983°E). (E) Top-to-the-NE asymmetric pressure shadow around K-feldspar porphyroblasts in augen gneiss from NE Song Chay dome indicating a top-to-the-NE sense of shear (22.909217°N, 104.8596°E). (F) microscopic photo of a mylonite from the Outer zone with Top-to-the-NE asymmetric pressure shadow around a quartz clast (22.643933°N, 105.8463°E).

Fig. 6. (A) Geological and structural map of the Ailaoshan belt (B-D) Cross sections through theSong Chay belt with locations marked in (A). (E-H) Stereographic projections of the foliations, and lineations and beddings for the

ophiolitic mélange zone, Ailaoshan group and sedimentary rocks from both Indochina and South China block (N: number of the measurements; Schmidt net, lower hemisphere).

Fig. 7. Field and micro-scale photographs of Ailaoshan belt. (A) Isoclinal fold in the meta-siltstone in the Central Ailaoshan zone, indicating the Cenozoic SW-ward thrust (24.66385°N, 100.89037°E). (B) Intensively cleavaged Late Triassic siltstone-mudstone in the Central Ailaoshan zone (23.982551°N, 101.375731°E). (C) Highly sheared quartz schist indicating a top-to-the-NE shearing in the Central Ailaoshan zone (24.686735°N, 100.913715°E). (D) Highly sheared quartz schist indicating a top-to-the-SW shearing in the Central Ailaoshan zone (23.5033°N, 101.8493°E). (E) Cleavaged pillow basalt in the Western Ailaoshan zone (23.9457°N, 101.3915°E). (F) Microscopic photograph of a mylonite from the Central Ailaoshan zone with prophyroclast showing a top-to-the-NE shearing (23.7116°N, 101.6715°E).

Fig. 8. Microphotograph of the chosen samples for quartz c-axis fabric analysis from different tectonic units to show the kinematics and related texture. (A) Bulging (BLG) and subgrain rotation (SGR) recrystallization and undulatory extinction in quartz grains, microfractures in plagioclase grains. (B) Bulging (BLG) and elongated quartz grains, with undeformed garnet suggesting a top-to-the-NE shearing. (C) Elongated quartz ribbon with bulging (BLG) and subgrain rotation (SGR) recrystallization. (D, E and F) Elongated quartz prophyroclasts in fine-grained matrix showing bulging (BLG) and subgrain rotation (SGR) recrystallization. (G and H) Undeformed plagioclase prophyroclasts, with bulging (BLG) subgrain rotation (SGR) recrystallization in quartz grains. (I, J and K) Bulging (BLG) recrystallization in elongated quartz grains. (L) Undeformed plagioclase and elongated quartz grains with bulging (BLG) subgrain rotation (SGR) recrystallization.

Fig. 9. Kinematic map of the Ailaoshan-Song Ma-Song Chay orogenic belt and quartz c axis diagrams measured by universal stage. Arrows point to the sense of shear of the upper layer over the lower layer. (Deformations related to Cenozoic RRF strike-slip are ignored; N: number of the measurements, Schmidt net, lower hemisphere).

Fig. 10. Field photographs and the Concordia diagrams of the samples for zircon U-Pb dating in Song Chay belt. The sample locations are marked in Figs. 2 and 4.

Fig. 11. $^{40}Ar/^{39}Ar$ age spectra on Muscovite from micaschist in the Inner zone of Song Chay belt. The sample locations are marked in Fig. 4.

Fig. 12. Geochronological constrains of Ailaoshan, Song Ma and Song Chay belt. 250-240 Ma represents the collision age of SCB and IB. The detail data are provided in the supporting material (Table S3).

Fig. 13. Crustal-scale interpretative tectonic model profiles of the Song Ma, Song Chay and Ailaoshan belt. Their locations were indicated in the Fig. 9.

Fig. 14. Complied ages of the ophiolitic mélanges of the three belts. The detail data are provided in the supporting material (Table S3).

Figure 15. A: Nowadays tectonic outline of SE Tibet; B: Middle-Late Triassic paleogeodynamic reconstruction of the Indochina -South China-Eastern Tibet area (modified from Faure et al., 2014).

Fig. 16. (A) Stratigraphic columns for the Indochina Block and South China Block (modified from Wang et al., 2018). (B) Complied published age data from three tectonic belts, the blue dots are the ages from three ophiolitic mélanges, the grey dots are the ages of magmatic rocks from the Western Ailaoshan-Truong Son magmatic belt, the orange dots are the $^{40}Ar/^{39}Ar$ ages or metamorphic zircon ages from the metamorphic rocks, the detailed data are provided in the supporting material (Table S3). (C) The evolutional model of Ailaoshan-Song Ma-Song Chay ocean.

Highlights

1. The linkage between Ailaoshan, Song Ma, and Song Chay tectonic belts was discussed
2. The $^{40}Ar/^{39}Ar$ ages reveal deformation age in the Song Chay belt between 250–245 Ma
3. Regional geochronological works constrain the evolution of Eastern Paleo-Tethys
4. Rifting-ocean spreading: 380–310 Ma, subduction: 310–250 Ma, collision: 250–240 Ma

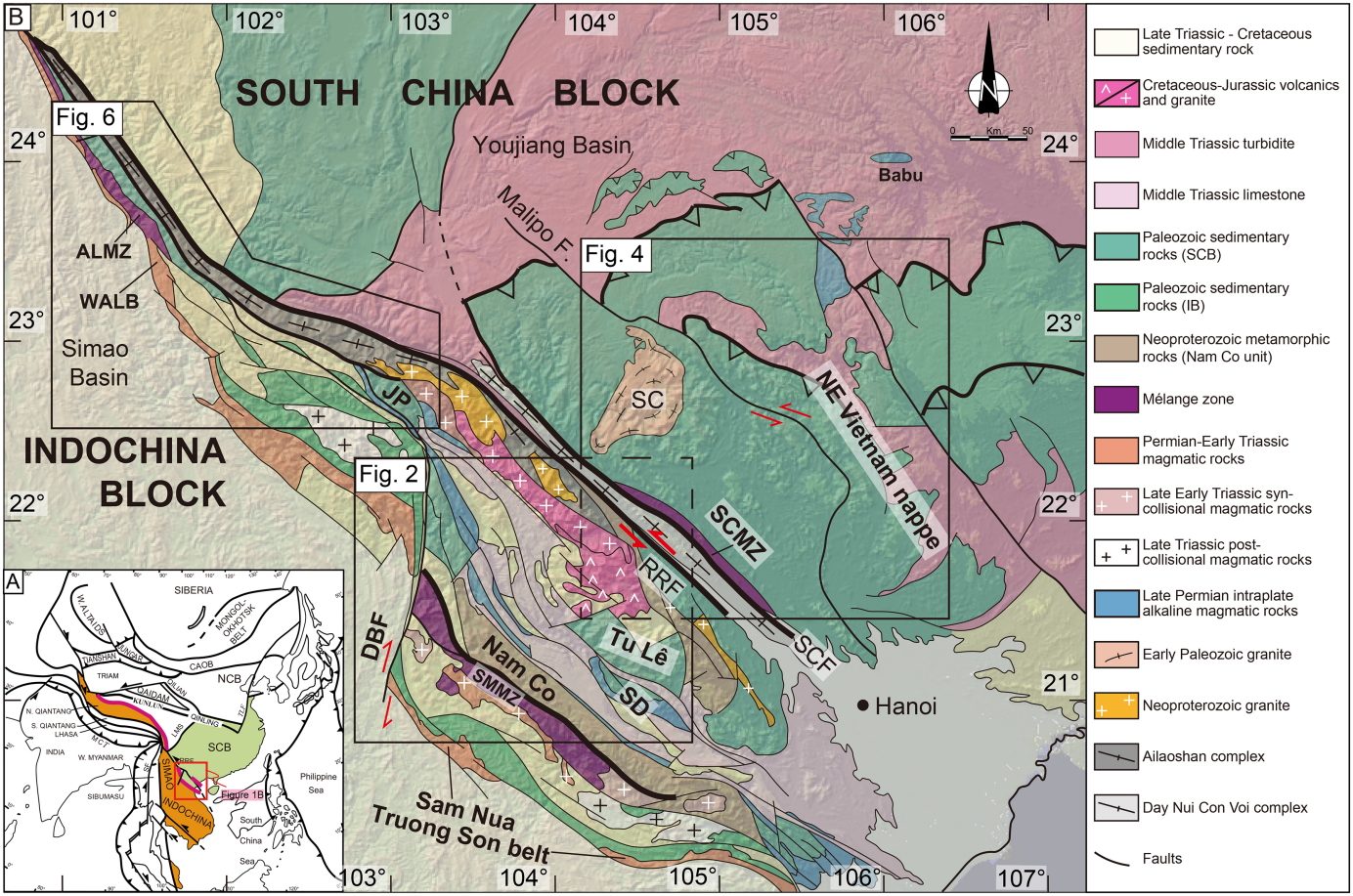

Late Triassic - Cretaceous sedimentary rock
Cretaceous-Jurassic volcanics and granite
Middle Triassic turbidite
Middle Triassic limestone
Paleozoic sedimentary rocks (SCB)
Paleozoic sedimentary rocks (IB)
Neoproterozoic metamorphic rocks (Nam Co unit)
Mélange zone
Permian-Early Triassic magmatic rocks
Late Early Triassic syn-collisional magmatic rocks
Late Triassic post-collisional magmatic rocks
Late Permian intraplate alkaline magmatic rocks
Early Paleozoic granite
Neoproterozoic granite
Ailaoshan complex
Day Nui Con Voi complex
Faults

Figure 1

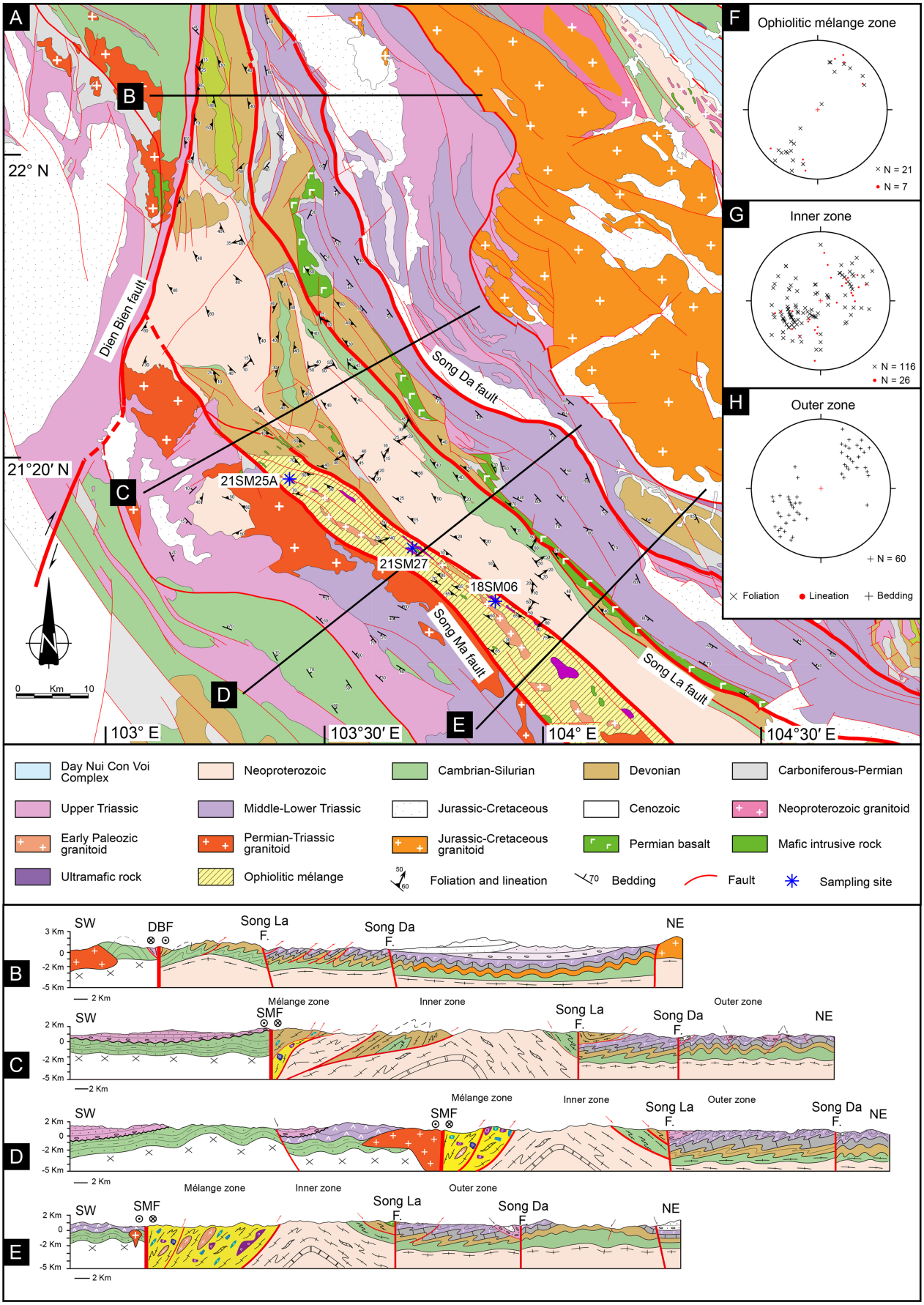
A
B
C
D
E
22° N
21°20′ N
103° E
103°30′ E
104° E
104°30′ E
Dien Bien fault
Song Da fault
Song Ma fault
Song La fault
21SM25A
21SM27
18SM06
0 Km 10
F
Ophiolitic mélange zone
× N = 21
• N = 7
G
Inner zone
× N = 116
• N = 26
H
Outer zone
+ N = 60
× Foliation
• Lineation
+ Bedding
Day Nui Con Voi Complex
Neoproterozoic
Cambrian-Silurian
Devonian
Carboniferous-Permian
Upper Triassic
Middle-Lower Triassic
Jurassic-Cretaceous
Cenozoic
Neoproterozoic granitoid
Early Paleozic granitoid
Permian-Triassic granitoid
Jurassic-Cretaceous granitoid
Permian basalt
Mafic intrusive rock
Ultramafic rock
Ophiolitic mélange
Foliation and lineation
Bedding
Fault
Sampling site
SW
DBF
Song La F.
Song Da F.
NE
3 Km
0
-2 Km
-5 Km
2 Km
Mélange zone
Inner zone
Outer zone
SMF

Figure 2

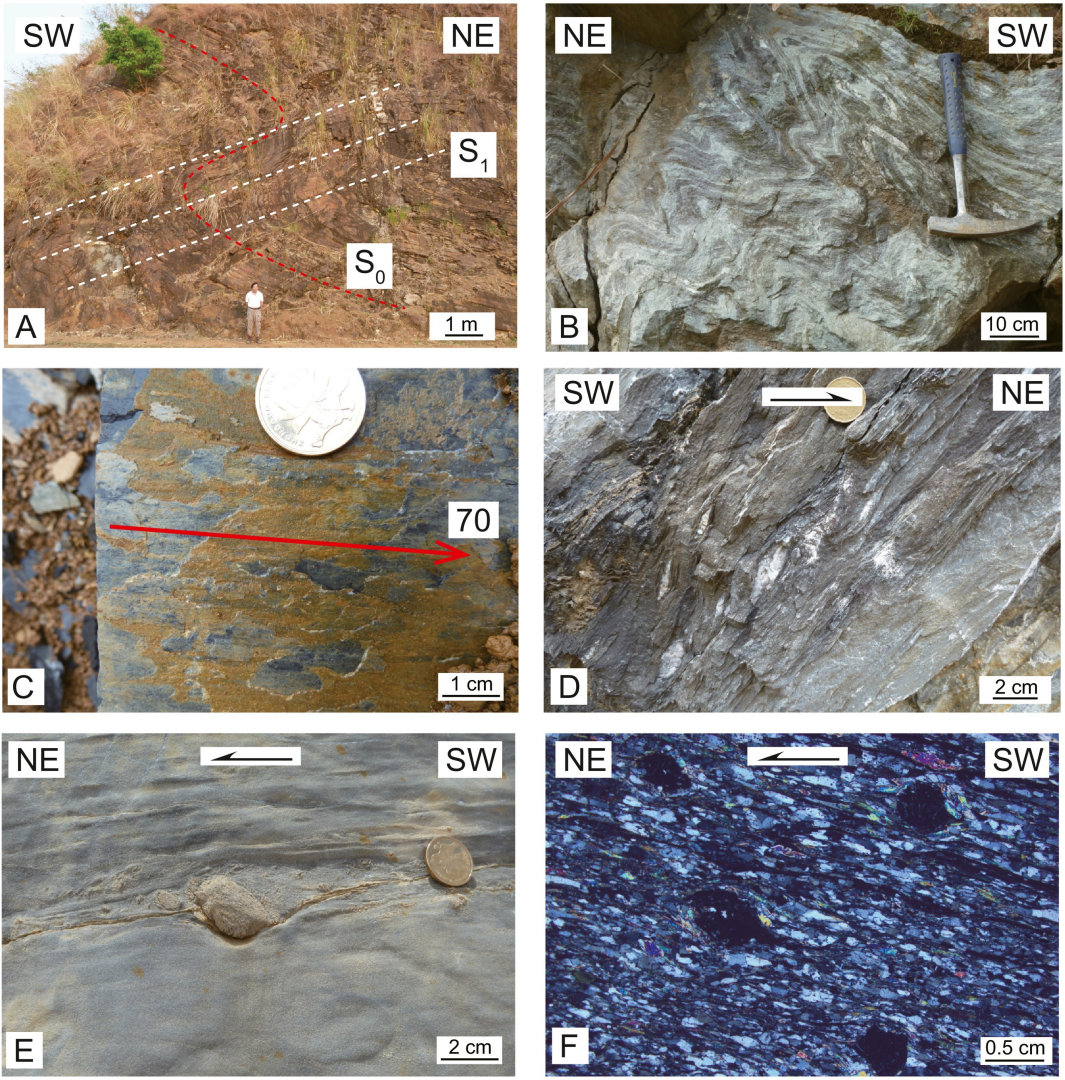
SW
NE
S_1
S_0
A
1 m
NE
SW
B
10 cm
70
C
1 cm
SW
NE
D
2 cm
NE
SW
E
2 cm
NE
SW
F
0.5 cm

Figure 3

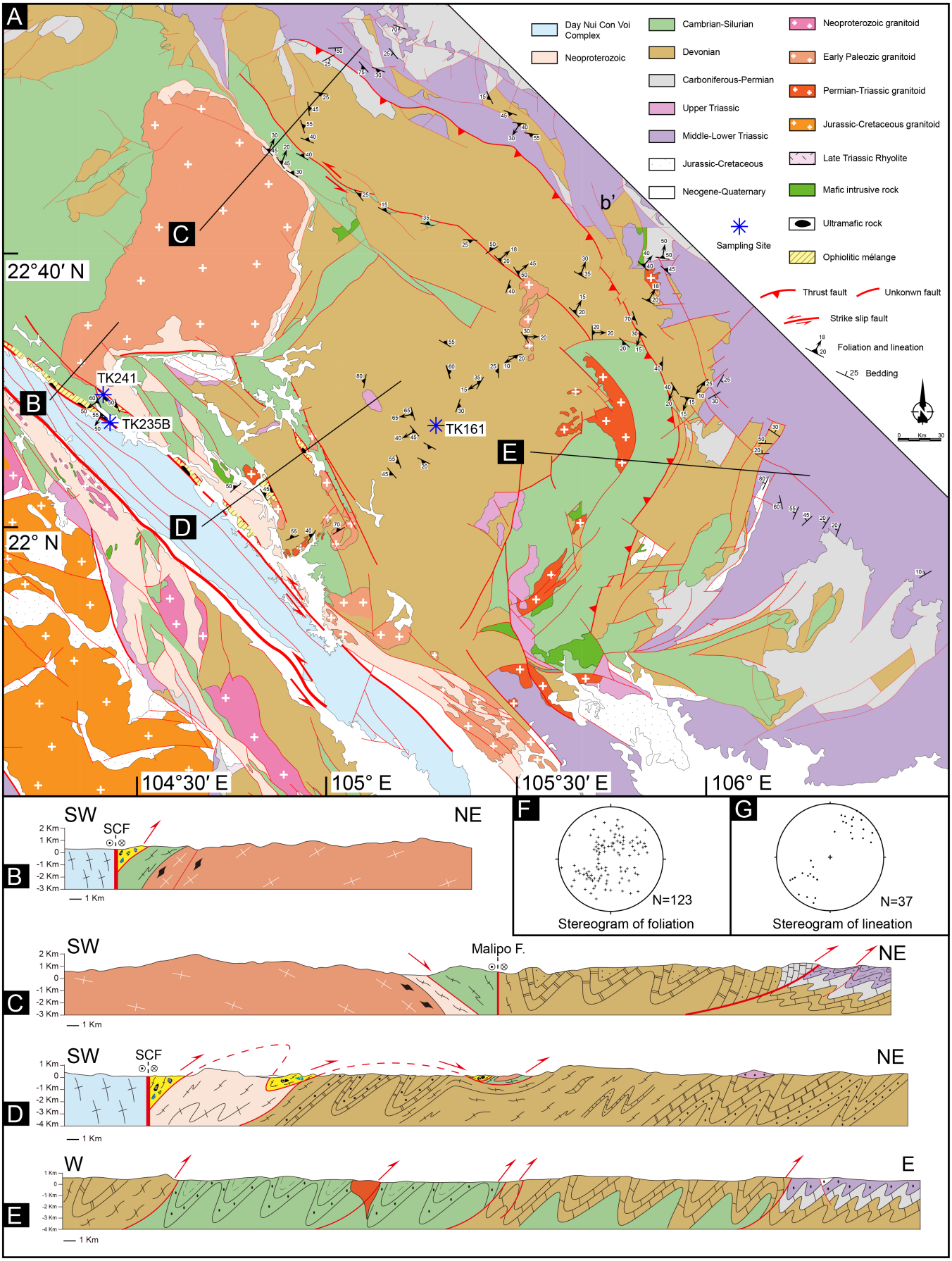
A
Day Nui Con Voi Complex
Neoproterozoic
Cambrian-Silurian
Devonian
Carboniferous-Permian
Upper Triassic
Middle-Lower Triassic
Jurassic-Cretaceous
Neogene-Quaternary
Neoproterozoic granitoid
Early Paleozic granitoid
Permian-Triassic granitoid
Jurassic-Cretaceous granitoid
Late Triassic Rhyolite
Mafic intrusive rock
Ultramafic rock
Ophiolitic mélange
Sampling Site
Thrust fault
Unkonwn fault
Strike slip fault
Foliation and lineation
Bedding
22°40′ N
22° N
104°30′ E
105° E
105°30′ E
106° E
TK241
TK235B
TK161
B
C
D
E
b'
SW
NE
SCF
2 Km
1 Km
0
-1 Km
-2 Km
-3 Km
1 Km
F
N=123
Stereogram of foliation
G
N=37
Stereogram of lineation
Malipo F.
-4 Km
W
E

Figure 4

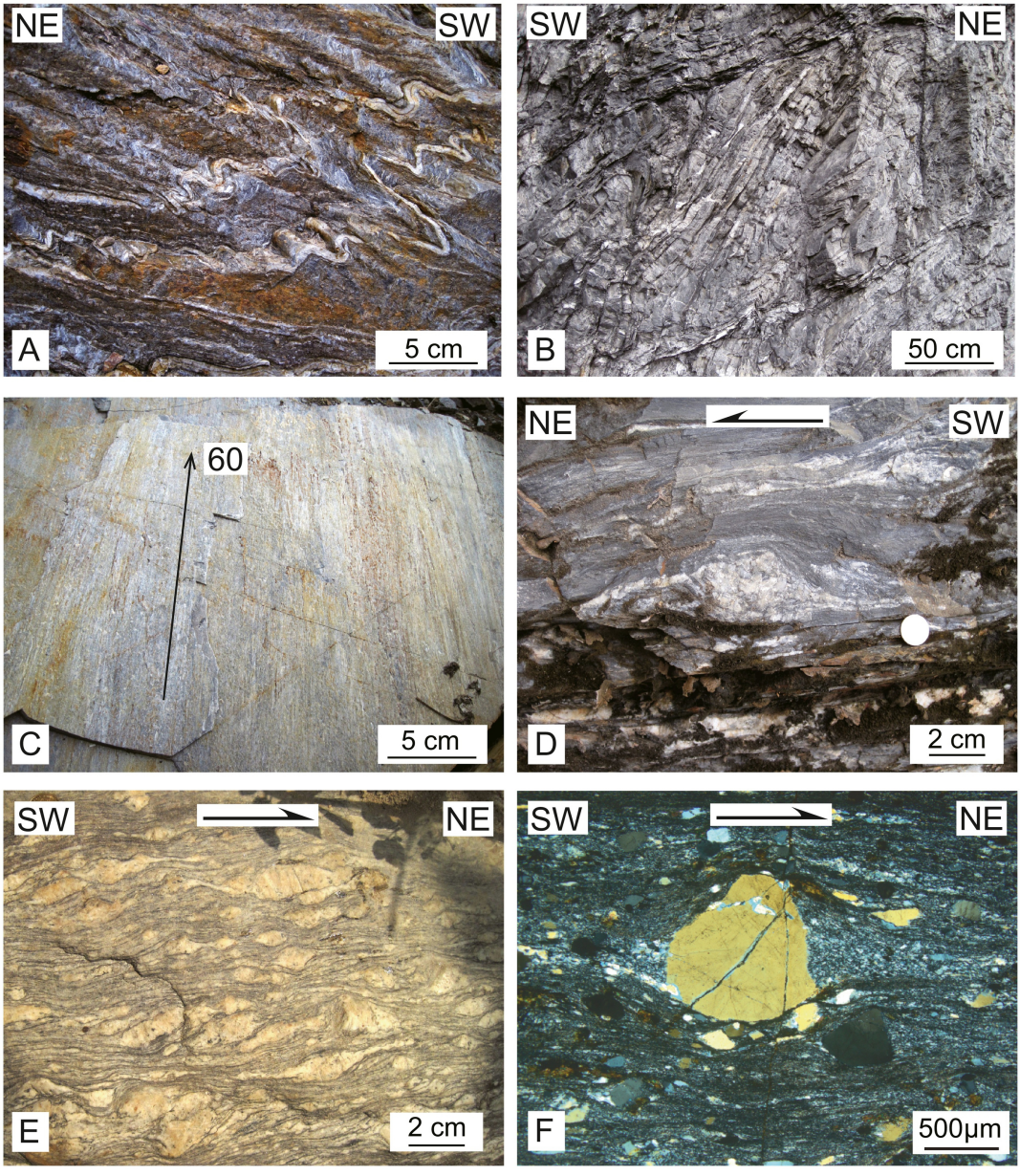

Figure 5

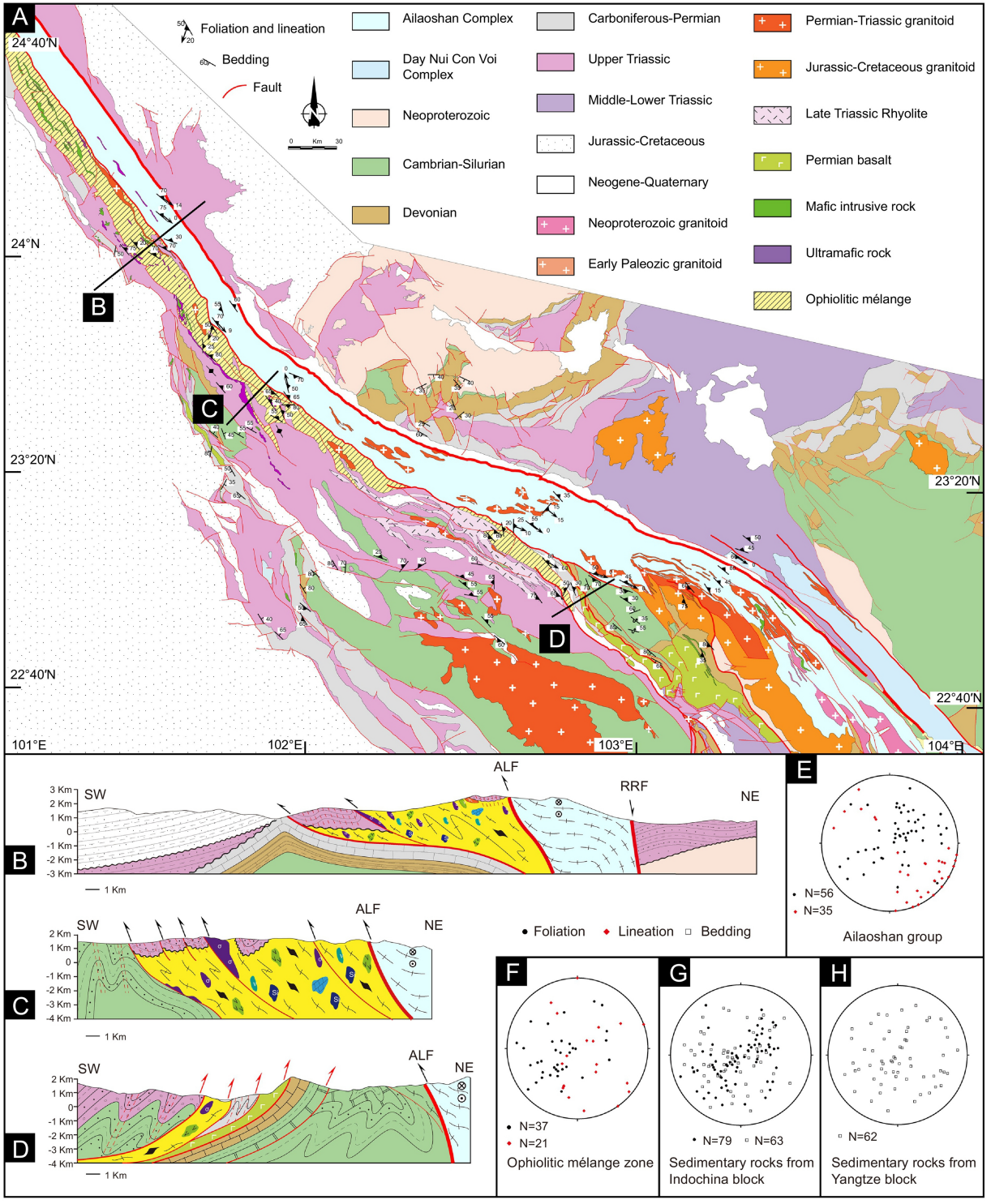
A
24°40'N
24°N
23°20'N
22°40'N
101°E
102°E
103°E
104°E
Foliation and lineation
Bedding
Fault
0 Km 30
Ailaoshan Complex
Day Nui Con Voi Complex
Neoproterozoic
Cambrian-Silurian
Devonian
Carboniferous-Permian
Upper Triassic
Middle-Lower Triassic
Jurassic-Cretaceous
Neogene-Quaternary
Neoproterozoic granitoid
Early Paleozic granitoid
Permian-Triassic granitoid
Jurassic-Cretaceous granitoid
Late Triassic Rhyolite
Permian basalt
Mafic intrusive rock
Ultramafic rock
Ophiolitic mélange
B
C
D
SW
NE
ALF
RRF
3 Km
2 Km
1 Km
0
-1 Km
-2 Km
-3 Km
-4 Km
1 Km
Foliation
Lineation
Bedding
E
N=56
N=35
Ailaoshan group
F
N=37
N=21
Ophiolitic mélange zone
G
N=79
N=63
Sedimentary rocks from Indochina block
H
N=62
Sedimentary rocks from Yangtze block

Figure 6

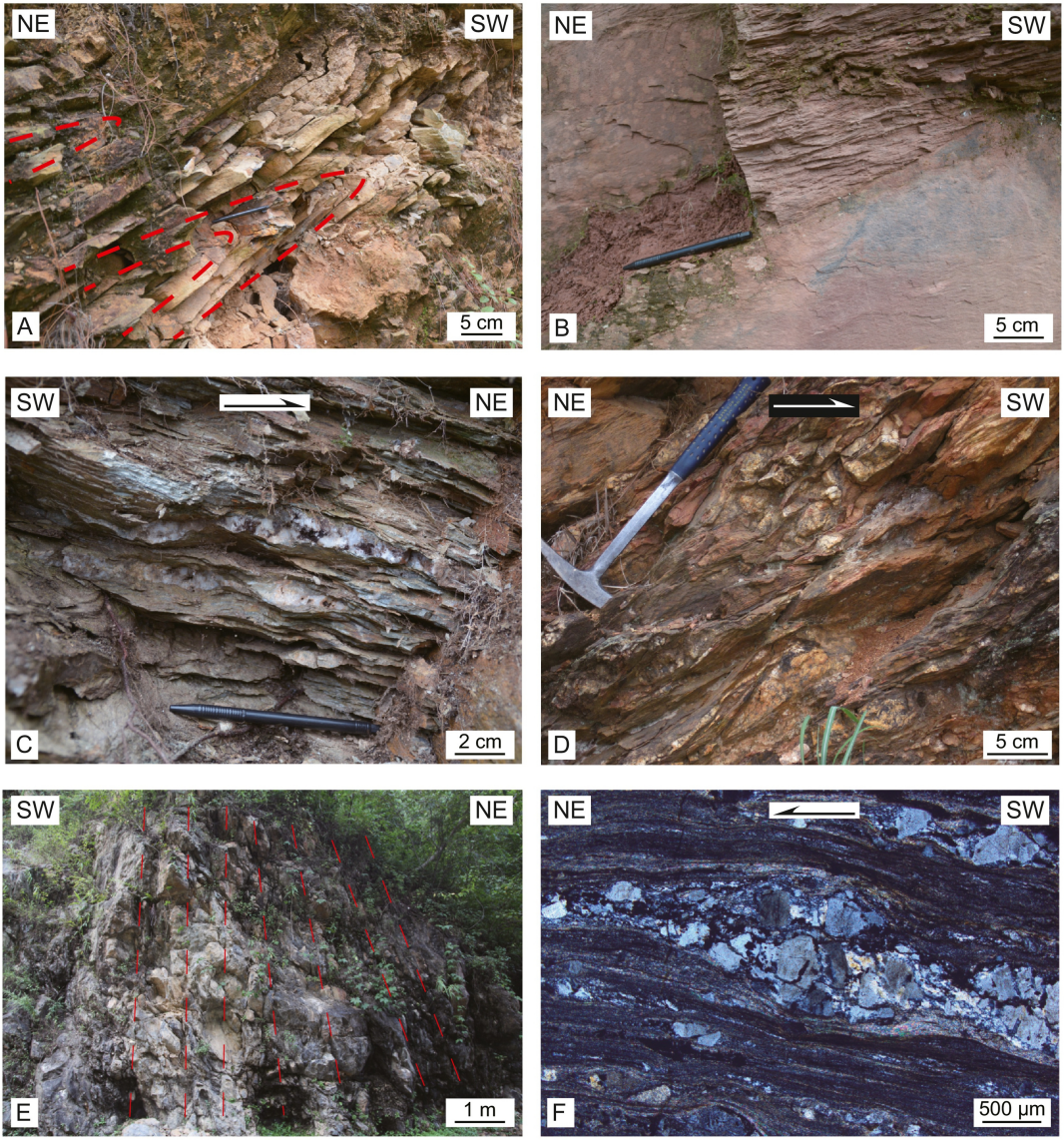

Figure 7

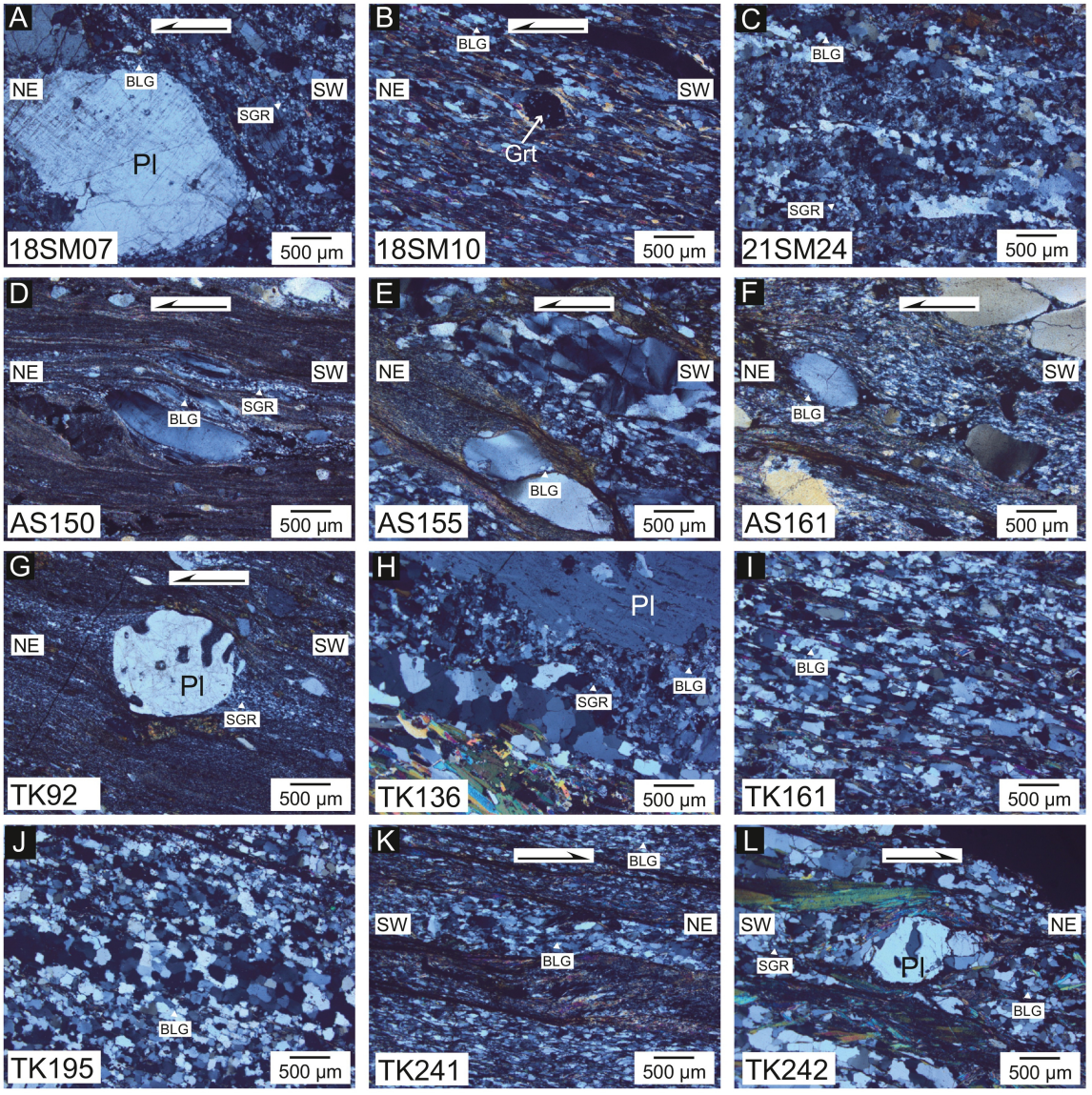
A
NE
BLG
SW
SGR
Pl
18SM07
500 µm
B
BLG
NE
SW
Grt
18SM10
500 µm
C
BLG
SGR
21SM24
500 µm
D
NE
SW
BLG
SGR
AS150
500 µm
E
NE
SW
BLG
AS155
500 µm
F
NE
SW
BLG
AS161
500 µm
G
NE
SW
Pl
SGR
TK92
500 µm
H
Pl
SGR
BLG
TK136
500 µm
I
BLG
TK161
500 µm
J
BLG
TK195
500 µm
K
BLG
SW
NE
BLG
TK241
500 µm
L
SW
NE
SGR
Pl
BLG
TK242
500 µm

Figure 8

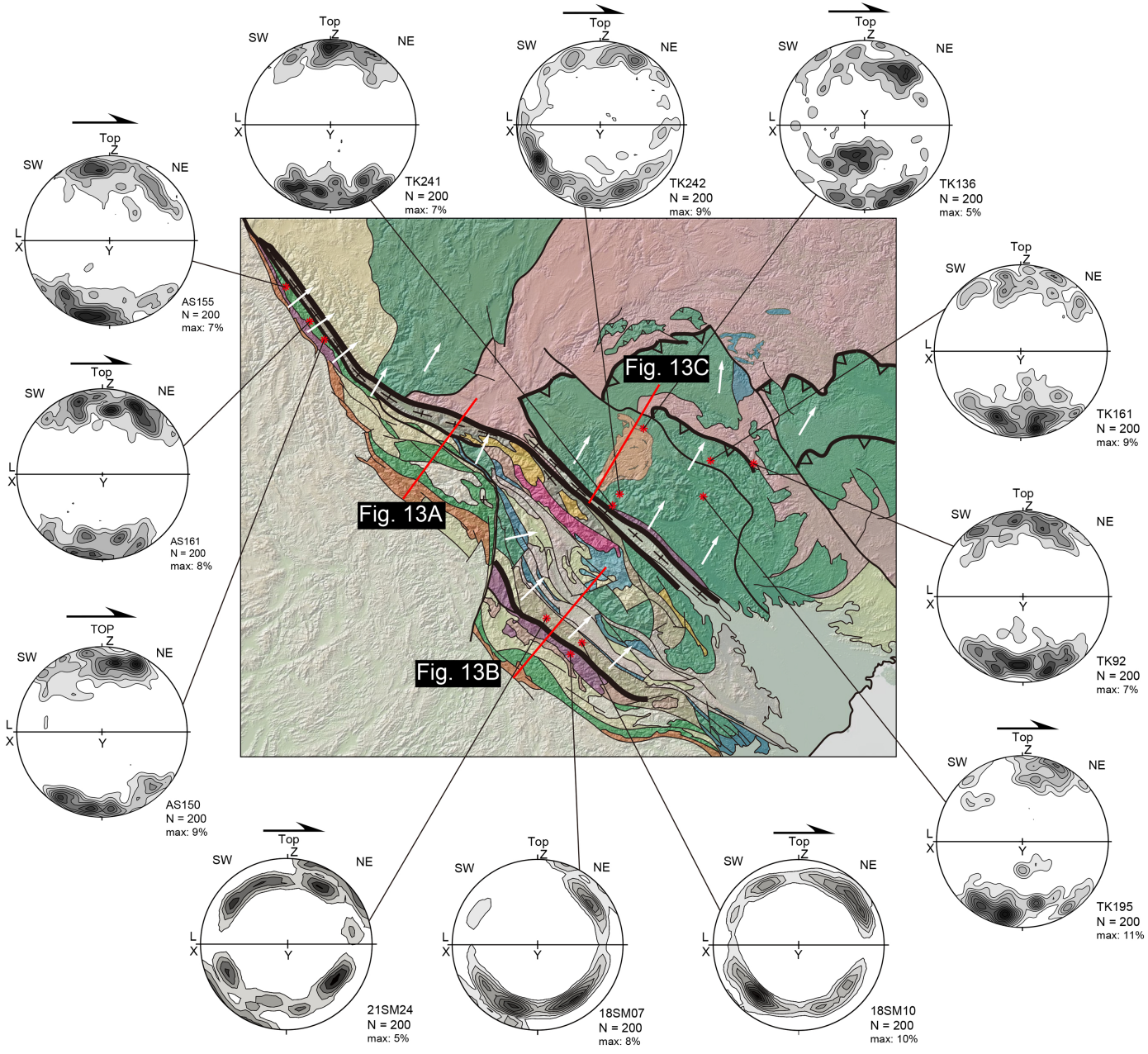
Top
SW
NE
Z
L
X
Y
TK241
N = 200
max: 7%
TK242
N = 200
max: 9%
TK136
N = 200
max: 5%
AS155
N = 200
max: 7%
TK161
N = 200
max: 9%
AS161
N = 200
max: 8%
TK92
N = 200
max: 7%
TOP
AS150
N = 200
max: 9%
TK195
N = 200
max: 11%
21SM24
N = 200
max: 5%
18SM07
N = 200
max: 8%
18SM10
N = 200
max: 10%
Fig. 13A
Fig. 13B
Fig. 13C

Figure 9

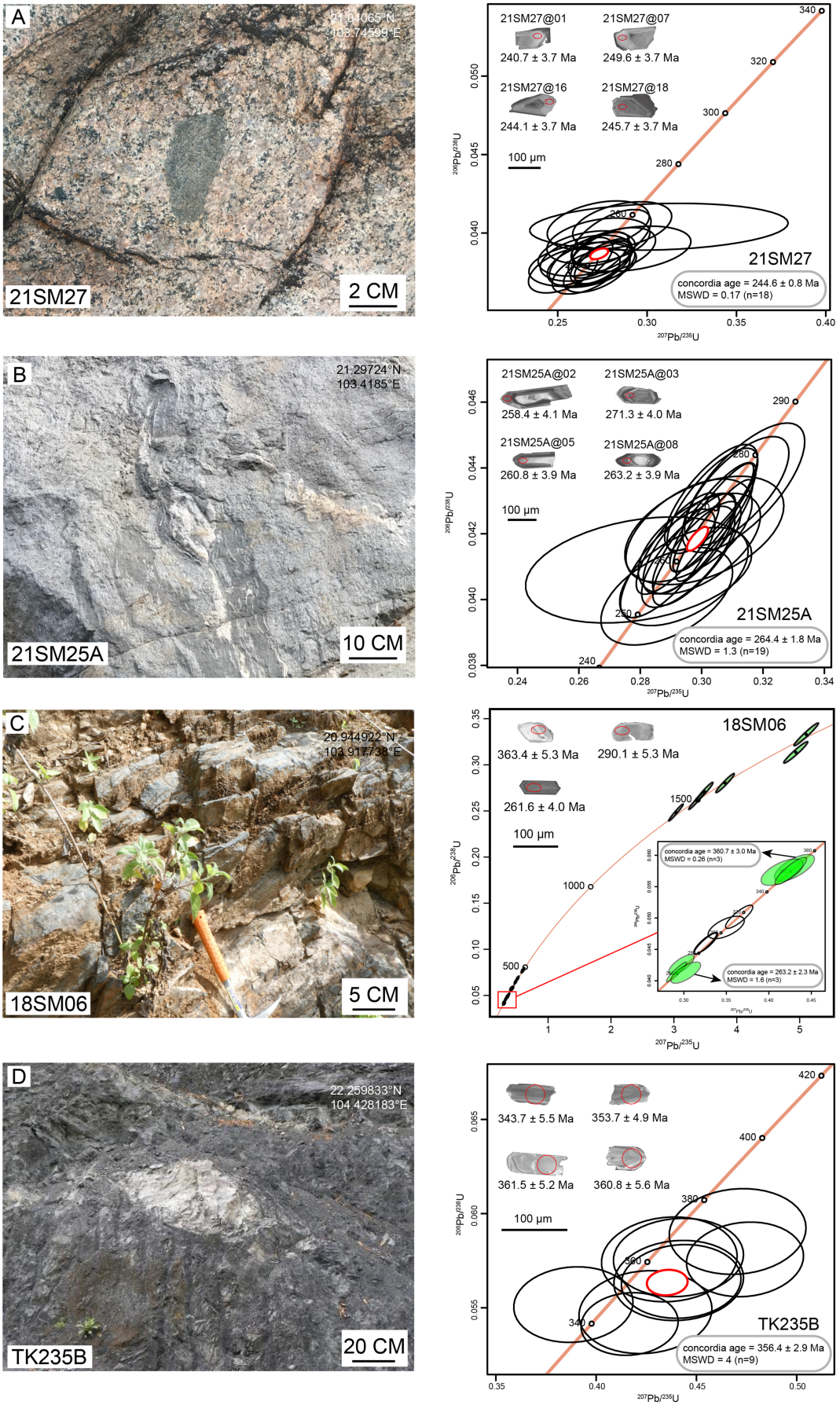
A
21.04065°N
103.74599°E
21SM27
2 CM
21SM27@01
240.7 ± 3.7 Ma
21SM27@07
249.6 ± 3.7 Ma
21SM27@16
244.1 ± 3.7 Ma
21SM27@18
245.7 ± 3.7 Ma
100 µm
21SM27
concordia age = 244.6 ± 0.8 Ma
MSWD = 0.17 (n=18)
B
21.29724°N
103.4185°E
21SM25A
10 CM
21SM25A@02
258.4 ± 4.1 Ma
21SM25A@03
271.3 ± 4.0 Ma
21SM25A@05
260.8 ± 3.9 Ma
21SM25A@08
263.2 ± 3.9 Ma
100 µm
21SM25A
concordia age = 264.4 ± 1.8 Ma
MSWD = 1.3 (n=19)
C
20.944922°N
103.917738°E
18SM06
5 CM
363.4 ± 5.3 Ma
290.1 ± 5.3 Ma
261.6 ± 4.0 Ma
100 µm
18SM06
concordia age = 360.7 ± 3.0 Ma
MSWD = 0.26 (n=3)
concordia age = 263.2 ± 2.3 Ma
MSWD = 1.6 (n=3)
D
22.259833°N
104.428183°E
TK235B
20 CM
343.7 ± 5.5 Ma
353.7 ± 4.9 Ma
361.5 ± 5.2 Ma
360.8 ± 5.6 Ma
100 µm
TK235B
concordia age = 356.4 ± 2.9 Ma
MSWD = 4 (n=9)

Figure 10

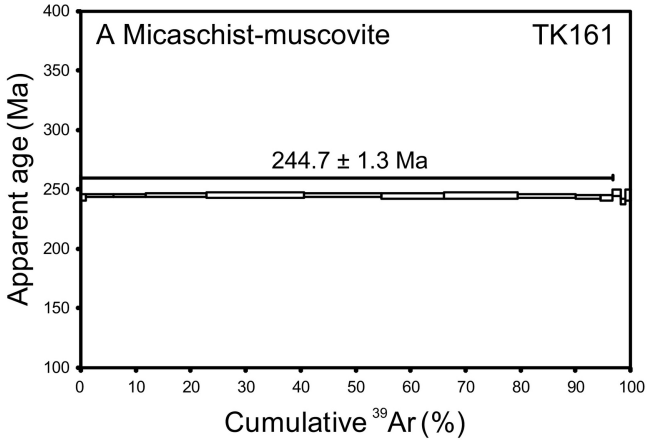
A Micaschist-muscovite
TK161
244.7 ± 1.3 Ma
Apparent age (Ma)
Cumulative ^{39}Ar (%)

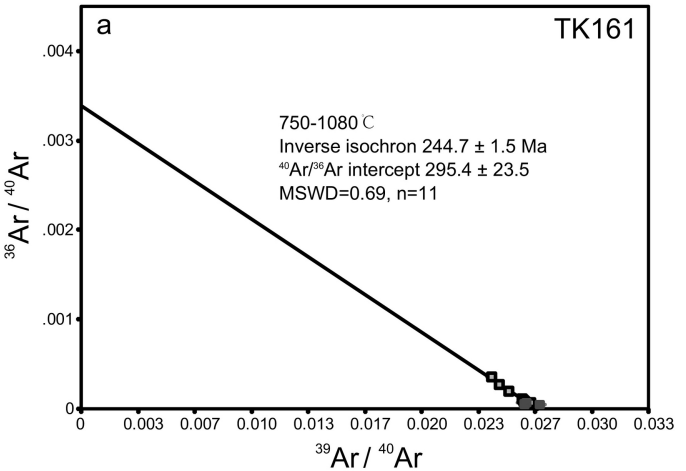
a
TK161
750-1080℃
Inverse isochron 244.7 ± 1.5 Ma
^{40}Ar/^{36}Ar intercept 295.4 ± 23.5
MSWD=0.69, n=11
^{36}Ar / ^{40}Ar
^{39}Ar / ^{40}Ar

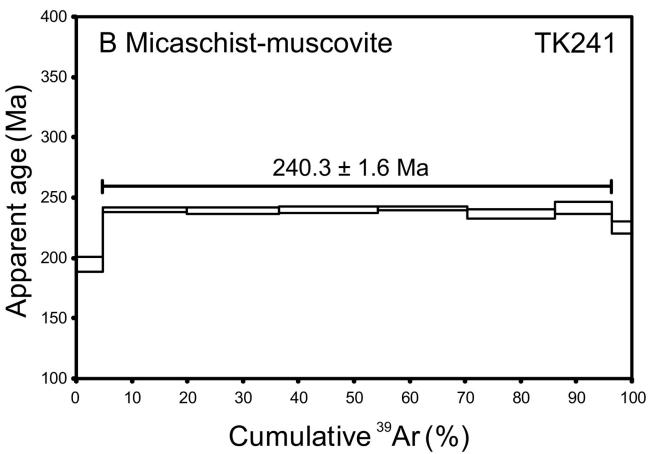
B Micaschist-muscovite
TK241
240.3 ± 1.6 Ma
Apparent age (Ma)
Cumulative ^{39}Ar (%)

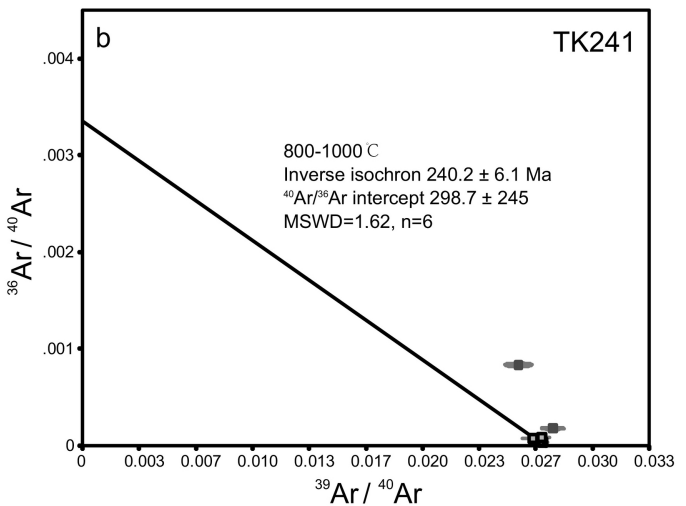
b
TK241
800-1000℃
Inverse isochron 240.2 ± 6.1 Ma
^{40}Ar/^{36}Ar intercept 298.7 ± 245
MSWD=1.62, n=6
^{36}Ar / ^{40}Ar
^{39}Ar / ^{40}Ar

Figure 11

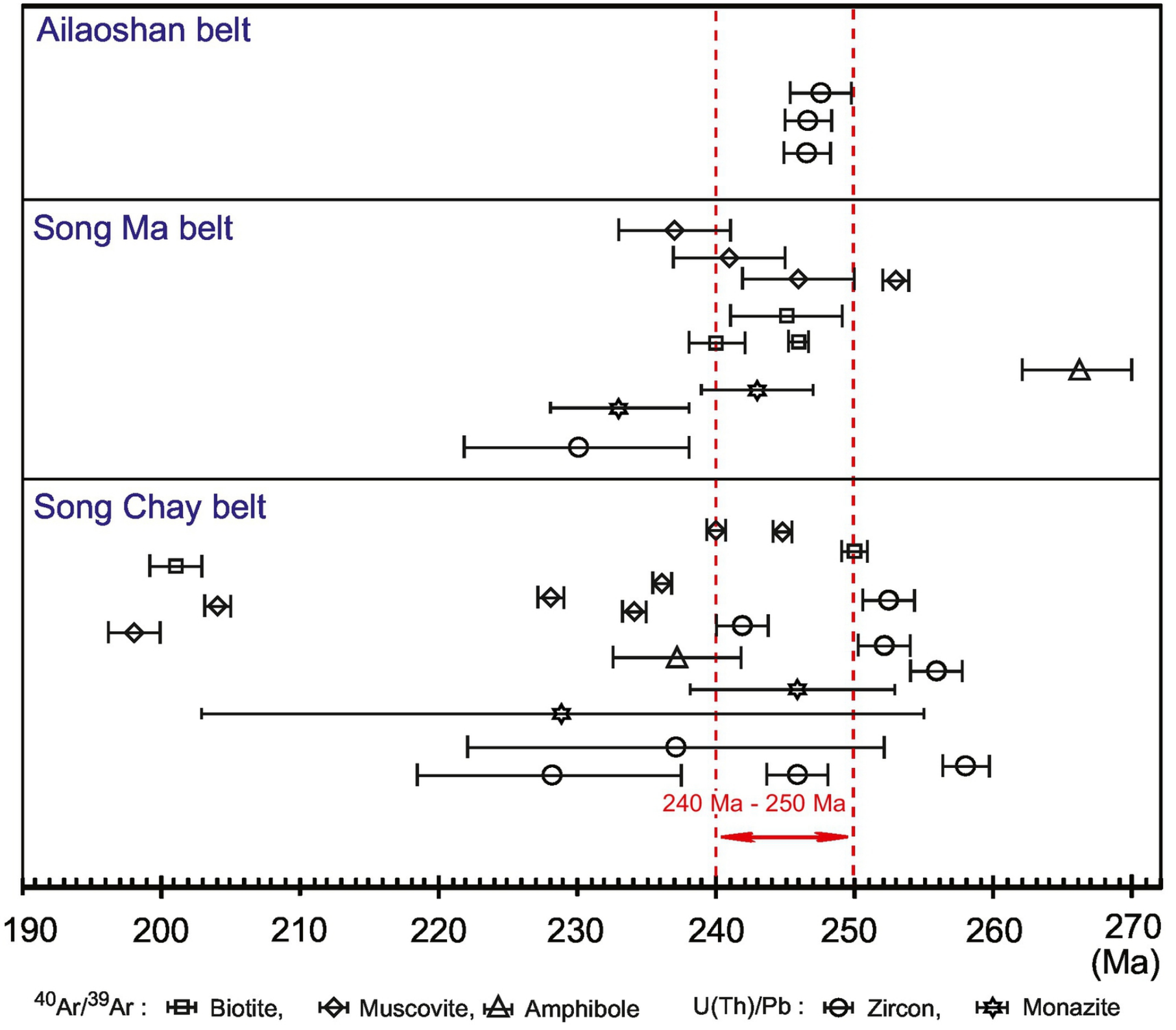
Ailaoshan belt
Song Ma belt
Song Chay belt
240 Ma - 250 Ma
190
200
210
220
230
240
250
260
270
(Ma)
40Ar/39Ar : Biotite, Muscovite, Amphibole
U(Th)/Pb : Zircon, Monazite

Figure 12

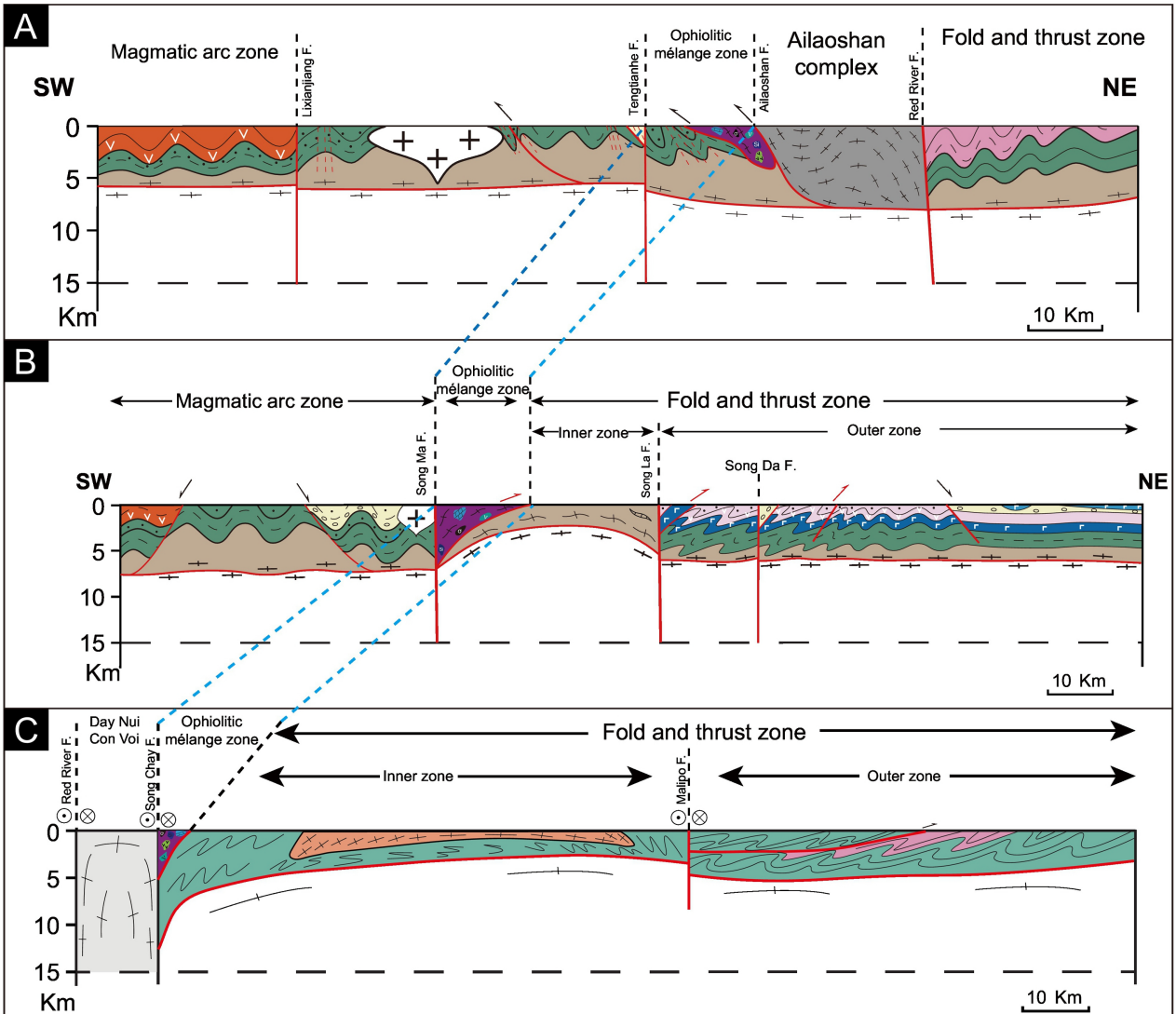
A
Magmatic arc zone
Lixianjiang F.
Tengtianhe F.
Ophiolitic mélange zone
Ailaoshan F.
Ailaoshan complex
Red River F.
Fold and thrust zone
SW
NE
0
5
10
15
Km
10 Km
B
Magmatic arc zone
Ophiolitic mélange zone
Fold and thrust zone
Inner zone
Outer zone
Song Ma F.
Song La F.
Song Da F.
SW
NE
0
5
10
15
Km
10 Km
C
Day Nui Con Voi
Ophiolitic mélange zone
Fold and thrust zone
Inner zone
Outer zone
Red River F.
Song Chay F.
Malipo F.
0
5
10
15
Km
10 Km

Figure 13

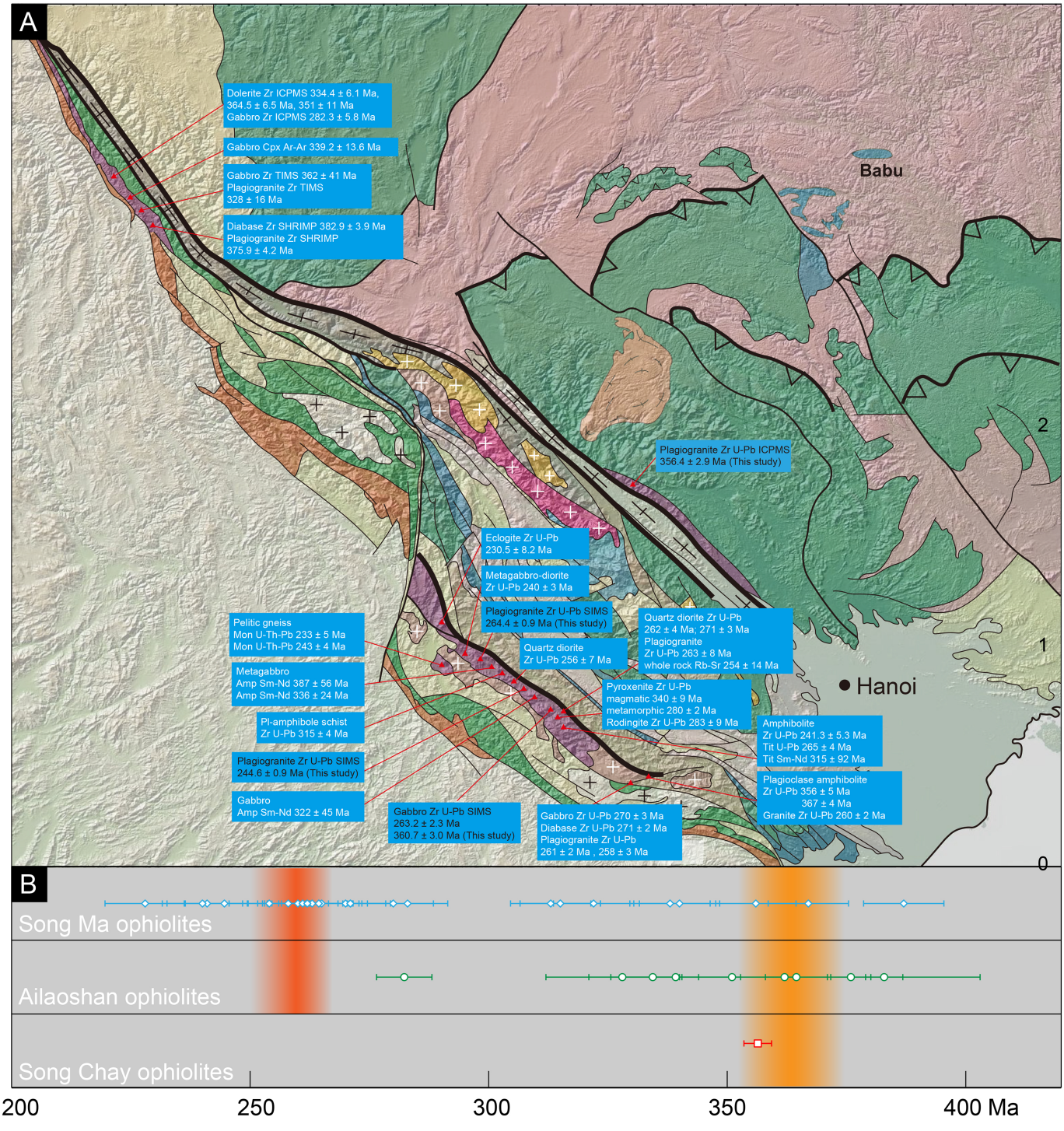
A
Dolerite Zr ICPMS 334.4 ± 6.1 Ma,
364.5 ± 6.5 Ma, 351 ± 11 Ma
Gabbro Zr ICPMS 282.3 ± 5.8 Ma
Gabbro Cpx Ar-Ar 339.2 ± 13.6 Ma
Gabbro Zr TIMS 362 ± 41 Ma
Plagiogranite Zr TIMS
328 ± 16 Ma
Diabase Zr SHRIMP 382.9 ± 3.9 Ma
Plagiogranite Zr SHRIMP
375.9 ± 4.2 Ma
Babu
Plagiogranite Zr U-Pb ICPMS
356.4 ± 2.9 Ma (This study)
Eclogite Zr U-Pb
230.5 ± 8.2 Ma
Metagabbro-diorite
Zr U-Pb 240 ± 3 Ma
Plagiogranite Zr U-Pb SIMS
264.4 ± 0.9 Ma (This study)
Quartz diorite Zr U-Pb
262 ± 4 Ma; 271 ± 3 Ma
Plagiogranite
Zr U-Pb 263 ± 8 Ma
whole rock Rb-Sr 254 ± 14 Ma
Pelitic gneiss
Mon U-Th-Pb 233 ± 5 Ma
Mon U-Th-Pb 243 ± 4 Ma
Quartz diorite
Zr U-Pb 256 ± 7 Ma
Metagabbro
Amp Sm-Nd 387 ± 56 Ma
Amp Sm-Nd 336 ± 24 Ma
Pyroxenite Zr U-Pb
magmatic 340 ± 9 Ma
metamorphic 280 ± 2 Ma
Rodingite Zr U-Pb 283 ± 9 Ma
Hanoi
Pl-amphibole schist
Zr U-Pb 315 ± 4 Ma
Amphibolite
Zr U-Pb 241.3 ± 5.3 Ma
Tit U-Pb 265 ± 4 Ma
Tit Sm-Nd 315 ± 92 Ma
Plagiogranite Zr U-Pb SIMS
244.6 ± 0.9 Ma (This study)
Plagioclase amphibolite
Zr U-Pb 356 ± 5 Ma
367 ± 4 Ma
Granite Zr U-Pb 260 ± 2 Ma
Gabbro
Amp Sm-Nd 322 ± 45 Ma
Gabbro Zr U-Pb SIMS
263.2 ± 2.3 Ma
360.7 ± 3.0 Ma (This study)
Gabbro Zr U-Pb 270 ± 3 Ma
Diabase Zr U-Pb 271 ± 2 Ma
Plagiogranite Zr U-Pb
261 ± 2 Ma , 258 ± 3 Ma
2
1
0
B
Song Ma ophiolites
Ailaoshan ophiolites
Song Chay ophiolites
200
250
300
350
400 Ma

Figure 14

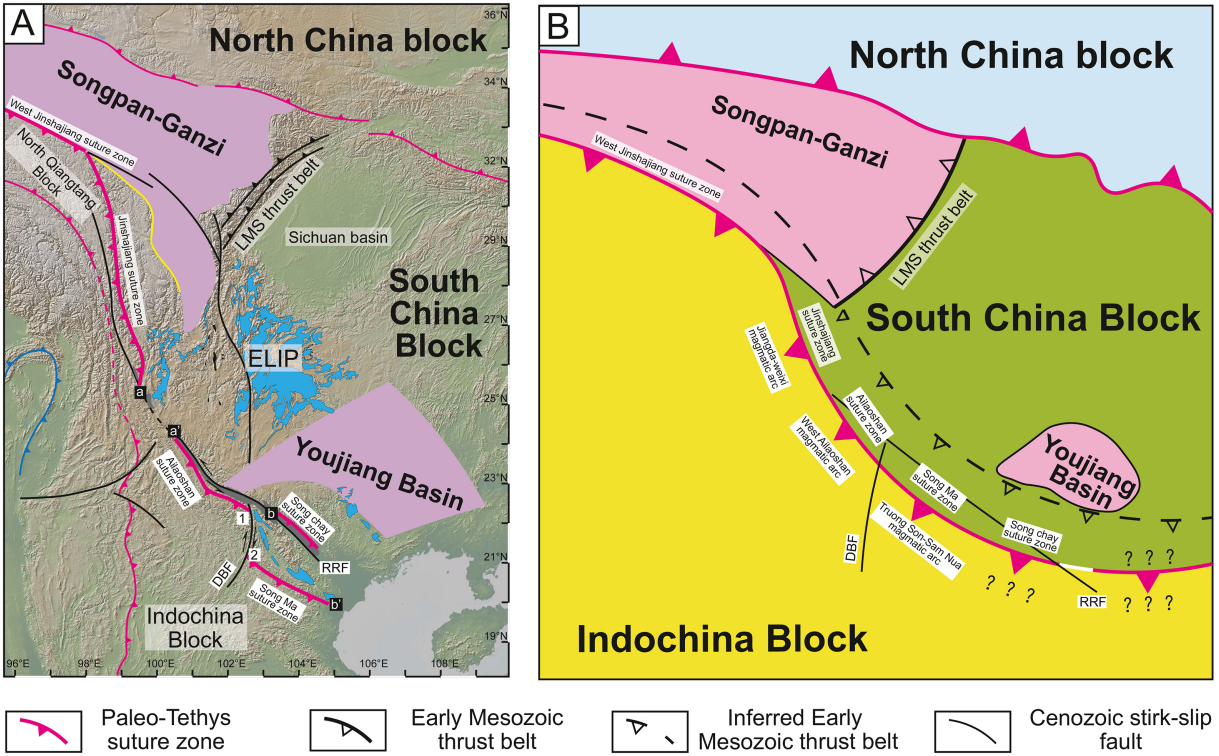
A
North China block
Songpan-Ganzi
West Jinshajiang suture zone
North Qiangtang Block
Jinshajiang suture zone
LMS thrust belt
Sichuan basin
South China Block
ELIP
Youjiang Basin
Indochina Block
Ailaoshan suture zone
Song chay suture zone
Song Ma suture zone
RRF
DBF
a
a'
b
b'
1
2
36°N
34°N
32°N
29°N
27°N
25°N
23°N
21°N
19°N
96°E
98°E
100°E
102°E
104°E
106°E
108°E
B
North China block
Songpan-Ganzi
West Jinshajiang suture zone
LMS thrust belt
South China Block
Jinshajiang suture zone
Jiangcang-weixi magmatic arc
Ailaoshan suture zone
West Ailaoshan magmatic arc
Youjiang Basin
Song Ma suture zone
Truong Son-Sam Nua magmatic arc
Song chay suture zone
DBF
RRF
? ? ?
? ? ?
? ? ?
Indochina Block
Paleo-Tethys suture zone
Early Mesozoic thrust belt
Inferred Early Mesozoic thrust belt
Cenozoic stirk-slip fault

Figure 15

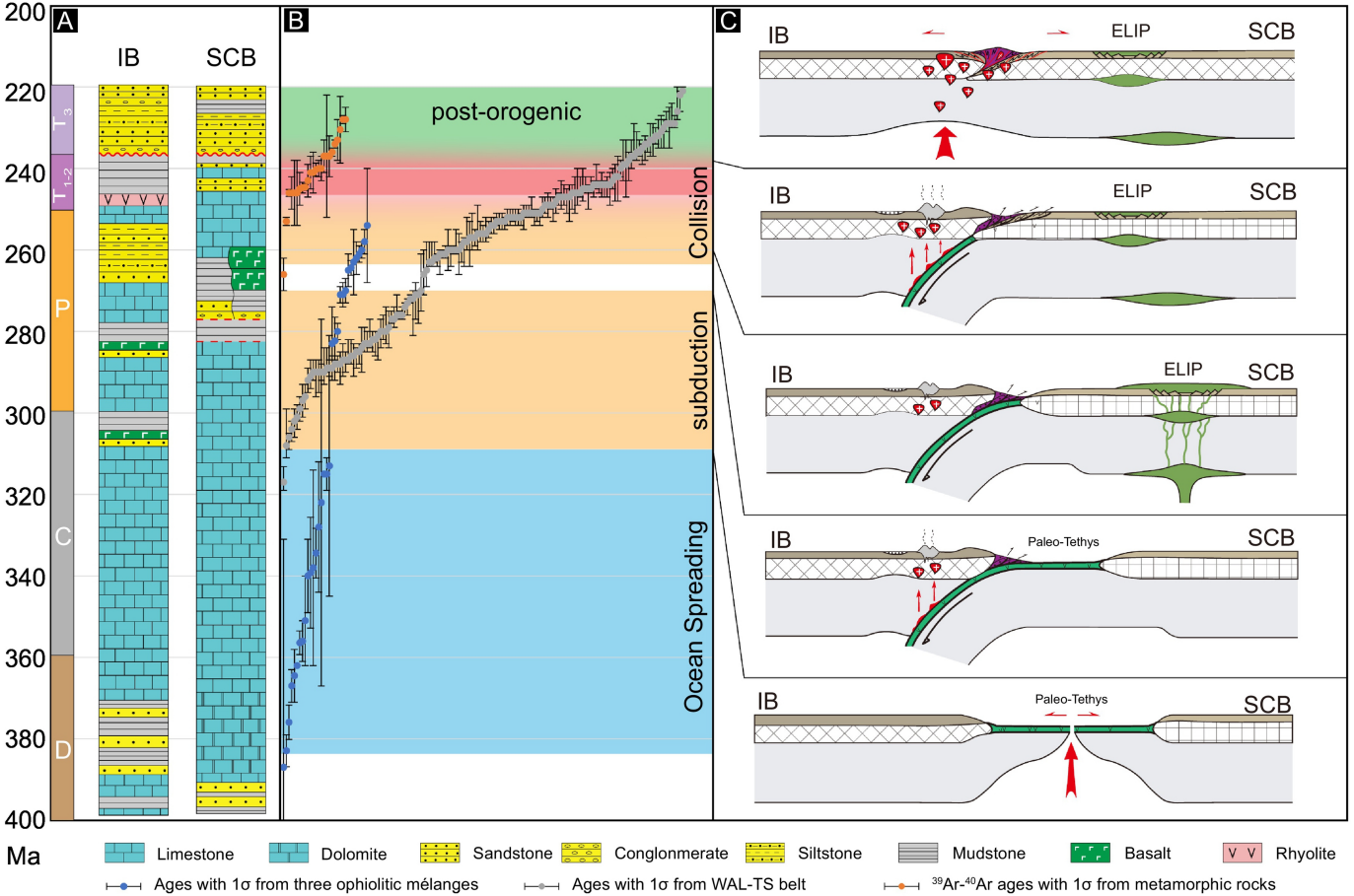
A
B
C
IB
SCB
post-orogenic
Collision
subduction
Ocean Spreading
ELIP
Paleo-Tethys
T3
T1-2
P
C
D
200
220
240
260
280
300
320
340
360
380
400
Ma
Limestone
Dolomite
Sandstone
Conglonmerate
Siltstone
Mudstone
Basalt
Rhyolite
Ages with 1σ from three ophiolitic mélanges
Ages with 1σ from WAL-TS belt
39Ar-40Ar ages with 1σ from metamorphic rocks

Figure 16